Clustering to characterize extreme marine conditions for the benthic region of the Northeastern Pacific continental margin

Amber M. Holdsworth[1], Andrew Shao[2], and James R. Christian[3]

[1]Fisheries and Oceans Canada -Institute of ocean Sciences
[2]Hewlett Packard Enterprise
[3]Fisheries and Oceans Canada

November 11, 2024

Clustering to characterize extreme marine conditions for the benthic region of the Northeastern Pacific continental margin

Amber M. Holdsworth[1], Andrew Shao[2], and James R. Christian[1,3]

[1]Fisheries and Oceans Canada
[2]Hewlett Packard Enterprise
[3]Canadian Centre for Climate Modelling and Analysis

Key Points:

- A generalizable method for characterizing ocean extremes was developed and applied to an Eastern Boundary Current environment.
- Climate indices are predictive of extreme conditions for the Northeastern Pacific continental margin.
- Multiple stressor extremes are rare, but are increasing in some regions, with most of involving compound extremes of oxygen and acidity.

Corresponding author: Amber M. Holdsworth, `Amber.Holdsworth@dfo-mpo.gc.ca`

Abstract

Anthropogenic CO_2 emissions lead to ocean warming, deoxygenation and acidification. Superimposed on the long-term trends are episodic extremes of temperature, oxygen, and acidity. Here we present an innovative method for assessing single and multiple stressor extremes using a high-resolution regional model of the Northeastern Pacific Ocean. We use an unsupervised clustering approach to identify regions with similar habitat characteristics near the seafloor, define extreme thresholds seasonally using a fixed baseline (1996-2020) within each cluster, and quantify the fraction of ocean waters that exceed these thresholds for both single and compound stressors. Compound extremes (most commonly of O_2 and acidification) are rare but show an increasing trend in some clusters. Potential predictability of occurrence of extremes is demonstrated by correlation with basin-scale climate variability.

Plain Language Summary

The ocean is becoming warmer, losing oxygen and acidifying as a result of CO_2 emissions. Superimposed on the mean changes are episodic extremes that can have detrimental impacts on ecosystems. To better understand the nature of extreme conditions on the continental margin, we use a statistical approach to characterize these extremes in the recent past (1996-2019).

We introduce a method for characterizing extremes that uses machine learning to divide the data into regions with relatively consistent environmental conditions (temperature, oxygen, acidity), and define the extremes based on the historical statistics of variability of each of these fields. For the Northeast Pacific continental margin, a substantial number of single stressor extremes occur annually. However, coincident extremes of more than one stressor are rare. Local extremes are related to large scale climate variability such as the North Pacific Gyre Oscillation. Long term trends are weak but detectable in some cases.

1 Introduction

Global warming, ocean deoxygenation, and acidification are inextricably linked. The ocean has taken up about 30% of anthropogenic carbon emissions and about 90% of the excess heat (Pörtner et al., 2019) which warms and acidifies the ocean and leads to deoxygenation through changes in solubility, stratification, ventilation, and respiration (Keeling et al., 2010; Breitburg et al., 2018). Ocean climate is changing rapidly and episodic extremes can drive changes in ecosystems decades before the mean state reaches that extreme.

Extremes of temperature, oxygen and acidity are projected to increase in the future (Kwiatkowski et al., 2020; Gruber et al., 2021). When these three stressors occur concurrently or consecutively they can have synergistic effects (Gruber, 2011) that impact organisms in ways that exceed the effects of a single stressor in isolation Pörtner et al. (2005). For example, increasing temperature can make species more sensitive to ocean acidification (Pörtner & Farrell, 2008), and oxygen and acidification can impact the thermal tolerances for some species (Pörtner, 2010). Some species will shift their distributions in response to these stressors (Thompson et al., 2023), while others will be unable to.

Episodic occurrences of anomalously warm ocean temperatures, known as marine heatwaves (MHW) have been associated with oxygen and acidification anomalies as solubility declines and stratification increases (Mogen et al., 2022). An analysis of satellite derived sea surface temperatures from the recent past (1982-2016) indicates that marine heatwaves (MHW) are increasing in duration and intensity. Earth system models

project increasing frequency, breadth, intensity and duration of MHWs (Frölicher et al., 2018). A doubling of impacts on species is anticipated by the 2050s (Cheung & Frölicher, 2020).

Marine heatwaves threaten marine life in the North Pacific and are associated with increasing occurrences of harmful algal blooms (Cavole et al., 2016), declines in the nutritional value of key forage fish (von Biela et al., 2019), reduction in stocks of commercially important fish (Cheung & Frölicher, 2020), mass mortality events, and loss of ecosystem services (Smale et al., 2019). The eastern North Pacific is one of the most productive regions in the world ocean (Cushing, 1971) and may be particularly vulnerable to biogeochemical extremes due to upwelling of waters that are low in oxygen and highly corrosive (primarily due to the age of the water). Corrosive ($\Omega_A < 1$) and hypoxic ($O_2 < 60\,\mathrm{mmol\,m^{-3}}$) water is projected to encroach on the Northeast Pacific continental margin by 2046-2065 (Holdsworth et al., 2021).

Previous studies have divided the shelf by defining bioregions using physical ocean variables and expert knowledge of the prevailing circulation (Zacharias et al., 1998). Rubidge et al. (2016) used machine learning to assimilate biological and environmental data to define ecoregions. They showed that the resulting ecological units represent more distinct species assemblages than the classifications based on expert knowledge. Clustering with machine learning reduces the need for personal interpretation or judgment by defining ecoregions using the data themselves.

This paper introduces a novel method for characterizing individual and compound extremes of temperature, oxygen, and acidification. The approach uses a clustering technique to establish subregions with similar environmental conditions and defines 'extreme' thresholds for upwelling and downwelling seasons using a fixed baseline. Assuming that extremes in these unique environmental spaces are influenced by similar processes helps disentangle the mechanistic drivers for this vast and complex region of the shelf. We use the method to analyze output from a high-resolution ocean biogeochemistry model of the Northeast Pacific from 1996 to 2019, restricting our analysis to the benthic layer of the Canadian coastal region, which contains unique ecosystems like glass sponge reefs and economically important shellfish and rockfish habitats. We then examine the occurrence of extreme conditions for both single and compound stressors.

Section 2 describes the regional model and the clustering technique; Section 3 discusses the spatial distribution of extreme thresholds and their evolution over time; Section 4 discusses these results in the broader context of extremes on continental margins and the utility of these findings to ecosystem management; lastly, Section 5 provides an overall summary of the paper and key results.

2 Methodology

2.1 Northeastern Pacific Ocean Model

The Northeastern Pacific (NEP) model domain spans the Canadian Pacific Ocean east of 140°W and north of 45°N (Figure 1 ab, Figure S1). The horizontal resolution is nominally 1/36° latitude and longitude which gives a variable grid spacing between 1.5 and 2.25 km. The model includes the ocean biogeochemistry module known as the Canadian Ocean Ecosystem model (CanOE) (Christian et al., 2022).

The regional ocean model, NEP36-CanOE, is an updated version of the one used in Holdsworth et al. (2021). We added a module for benthic remineralization and phytoplankton and zooplankton parameters (Figure S2) were adjusted to make the community more representative of the Northeastern Pacific continental margin. More details of the model configuration and development can be found in Text S1.

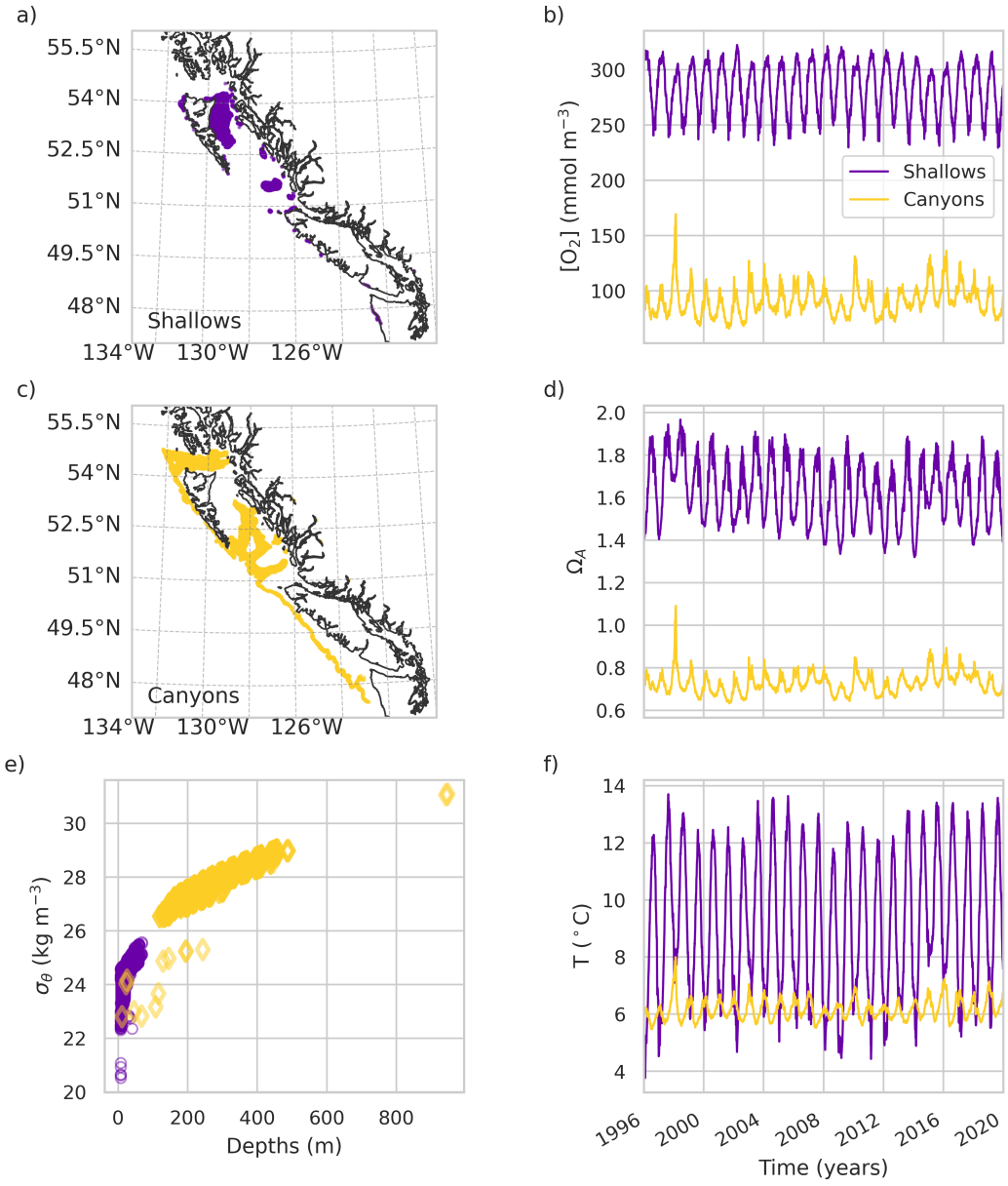

Figure 1. Maps of the (a) Shallows and (c) Canyons clusters with (e) density as a function of depth. Spatially averaged time-series of the daily averaged (b) dissolved oxygen, (d) aragonite saturation state, and f) potential temperature for each cluster. Geographic locations are labelled on Figure S1.

The model was forced with hourly atmospheric forcing from the ERA5 reanalysis (Hersbach et al., 2018); the metpy package was used to convert dew point and pressure to specific humidity (May et al., 2021). At the open boundaries we used the Copernicus Global 1/12° Oceanic and Sea Ice (GLORYS12) Reanalysis (Lellouche et al., 2021) for the physical variables, we used the Global Ocean Data Analysis Project version 2 (GLODAP) (Key et al., 2015; Lauvset et al., 2016) for dissolved inorganic carbon (DIC) and Total Alkalinity (TAlk), and World Ocean Atlas 2018 for nitrate plus nitrite (NO_3) and dissolved oxygen (O_2) (Garcia et al., 2019a, 2019b).

The model's grid spacing is insufficient to resolve locations very near to the shore as well as the narrow straits and channels along the coast. Therefore, we apply a mask to remove the 2 grid cells next to the coast and any channels less than 25 km wide which effectively removes the Salish Sea from our analysis (Figure S1).

The hindcast simulation was extensively evaluated using all of the available ship-sampled data (Department of Fisheries and Oceans Canada (DFO), 2022) (Figure S3), Monthly Isopycnal / Mixed-layer Ocean Climatology (MIMOC) (Schmidtko et al., 2013) (Figure S4), and tide gauge observations from 65 stations (Figure S5). More details of the evaluation can be found in supplementary Text S1. The model distributions are similar to those of the ship-sampled observations (Figure S3). We computed several metrics including the Kling-Gupta Efficiency (KGE) and its components (the Pearson correlation r, the variability ratio α, and the bias ratio β) (Kling et al., 2012; Jackson et al., 2019) as well as the signed root mean squared error (RMSE). All of the variables relevant to our analysis were strongly correlated with the observations and perform well compared to the mean observed benchmark (KGE < 0.75) (Table S2). To assess the capability of the simulation to represent extreme conditions, we computed the 10^{th} and the 90^{th} percentile from these distributions. Extreme values for T, S, DIC, TAlk and hypoxia have a relatively low bias (Table S2). Therefore, the simulation is expected to realistically represent extreme marine conditions for each of the three stressors.

2.2 Clustering methodology

The benthic Northeast Pacific is a heterogenous environment; spatial distribution of physical and biogeochemical properties is affected by topography and the large-scale circulation. Thus, a single definition for an extreme is not necessarily appropriate; what is a 'typical' value for one sub-region might be considered 'extreme' for another. Additionally, defining specific biomes using expert knowledge is challenging due to the complex circulation and the size of the study region. Instead, we use a clustering approach that provides a data driven estimate of regions where the three stressors respond similarly to changes in upwelling/downwelling, biogeochemistry, and circulation.

Clustering is a method used in machine learning to group similar data points together based on certain selected features or input variables. Since we are interested in characterizing T, $[O_2]$, and acidification extremes, the selected features are calculated climatologies of T, apparent oxygen utilization (AOU), and aragonite saturation state, Ω_A for all bottom depths less than 1000 m in the model. AOU is used instead of $[O_2]$ to eliminate the effect of solubility on oxygen concentration (which potentially overemphasizes T in defining a cluster). While ocean acidification can be considered a 'multiple driver' because multiple inorganic carbon parameters are changing (Hurd et al., 2019), we include only Ω_A as a variable with important biotic impacts. Each of these is scaled to have zero mean and unit standard deviation. A K-means clustering algorithm (Pedregosa et al., 2011) is then applied to these data to find six distinct clusters whose members have similar relationships among the three variables (Table S3 and Figure S6). Two choices that were made for this study are the number of clusters and the temporal resolution of the data. More details on how these choices were made are given in Text S2.

Visual examination of the clusters (Figure S6) shows that two (d, a) of the six are well-defined regions representing shallow shoals and submarine canyons, respectively (Figure 1 a, c) and referred to as Shallows and Canyons hereafter. We selected these two clusters for detailed analysis, based on their contrasting characteristics, and their ecological relevance; the Canyons and Shallows clusters both contain bioregions with high biodiversity (c.f. the Troughs and Dogfish Bank units in Rubidge et al. (2016) Figure 3). However, other clusters may also be of ecological interest, for example, cluster 'e' highlights regions of high species richness for groundfish (c.f. Figure 8 of Thompson et al. (2022)).

From the climatologies, we computed the center for each of the clusters (Table S3). The Shallows cluster has relatively warm temperatures, low AOU (high oxygen), and aragonite supersaturation, while the Canyons cluster has low T, high AOU, and undersaturation (Table S3).

Due to the changes in circulation and life stages of the biota, we examine daily output split into two seasons: an upwelling season (April to September) and a downwelling season (October to March). The boundary between these seasons is the average date of the spring and fall transitions (March 31^{st} and October 12^{th}) observed between 1991 and 2020 (Boldt et al., 2020).

2.3 Defining thresholds for extremes

To define a threshold for what is considered extreme, we rely on the statistics of daily average T, $[O_2]$, and Ω_A. Here we use $[O_2]$ instead of AOU, because biotic impacts are related to oxygen concentration.

We implement a relative threshold approach and define a fixed baseline for each regime using the full 24 year time series from January 1996 to December 2019 (Gruber et al., 2021). Because the distributions are asymmetric (complicating the definition of thresholds based on variance), we choose a percentile-based approach to identify thresholds. The thresholds are calculated from the cumulative density function (distributions shown in Figure S7) for each cluster using the 10^{th} percentile for Ω_A and $[O_2]$, and the 90^{th} percentile for T (Hobday et al., 2016; Gruber et al., 2021).

3 Results

3.1 Characterization of the clusters

The Shallows cluster (Figure 1 a) includes the open waters east of Haida Gwaii and some of the shallow banks in Queen Charlotte Sound. The Canyons cluster (Figure 1 b) includes the deep channels of Dixon Entrance north of Haida Gwaii, the troughs of Queen Charlotte Sound and connected waters along the edge of the continental shelf.

The Shallows and Canyons have contrasting environmental conditions. Each cluster displays a strong seasonal cycle (Figure 1 b-d-f); related to seasonal upwelling and downwelling. Compared to the Canyons (263 m average depth), the Shallows (30 m average depth) exhibits a higher seasonal amplitude, particularly for temperature. While this can be partly attributed to their average depth, some depths and isopycnals in the Shallows overlap with the Canyons, which spans a wider range (Figure 1 e).

The thresholds that define extreme conditions during each season, calculated using the criteria for each variable described in section 2.3, are show in Table 1. For the Canyons, an extreme value for O_2 is close to the widely used criterion for hypoxia that may signify fisheries collapse ($< 60\,\text{mmol}\,\text{m}^{-3}$) (Vaquer-Sunyer & Duarte, 2008), and is associated with aragonite undersaturation; for the Shallows, the oxygen threshold is well above the 'conservation limit' of $\simeq 140\,\text{mmol}\,\text{m}^{-3}$ and occurs in aragonite saturated

and relatively warm waters. In the Shallows, extreme temperatures occur during the summer months when atmospheric temperature is greatest; in the Canyons, warm extreme temperatures occur during downwelling (Table 1). Upwelling during summer brings relatively cool, salty, low oxygen and nutrient rich water to the deep benthic regions of the continental shelf; during winter, downwelling and mixing can propagate surface signals downward.

Table 1. The thresholds relative to 1996-2019 (section 2.3) and maximum duration (days) averaged over all of the grid cells within the cluster for extreme events of temperature (°C), dissolved oxygen (mmol m^{-3}) and aragonite saturation state for the Shallows (Figure 1a) and Canyons (Figure 1c) clusters.

Cluster	Upwelling Threshold			Downwelling Threshold			Upwelling max duration			Downwelling max duration		
	T	O_2	Ω_A	T	O_2	Ω_A	T	O_2	Ω_A	T	O_2	Ω_A
Shallows	14.1	241	1.5	10.7	260	1.3	3.4	4.2	6.3	2.5	4.2	6.2
Canyons	6.4	59	0.6	7.1	69	0.6	6.7	6.3	5.4	7.7	7.0	5.6

3.2 Occurrence of extremes over time

In the Canyons, two time periods (1999-2003 and 2008-2013) have a large fraction of waters ($> 40\%$) with extreme values of $[O_2]$ and Ω_A (Figure 2 a, b). These time periods correspond to the positive phase of the North Pacific Gyre Oscillation (NPGO). For temperature, the largest fraction of extreme waters ($> 50\%$) occurs during downwelling in 1998, and during upwelling in 2010, 2016 and 2019.

In the shallows, up to 80% of waters experience extreme conditions for $[O_2]$ in 1998 during a very strong El Niño and in 2014 during the MHW. The most extreme conditions for Ω_A occurred during the upwelling season of 2009 (Figure3).

For $[O_2]$ and T, the most extreme conditions tend to occur at the beginning of the downwelling season when atmospheric temperatures are warmest. While this is partly an artifact of having seasonally defined thresholds, it reflects the interannual variability in the time series.

With the exception of an increase in Ω_A extremes in the Shallows (0.004 y^{-1}) , neither cluster exhibits a linear trend in the percentage of extremes (Figures 2, 3, and Text S3). For the Canyons, this may be because the upwelled waters are old and do not contain a signature of recent anthropogenic climate change. In the shallows there may be a trend associated with increasing surface air temperature, but this is damped somewhat by mixing with subsurface waters. In any case, the timescale of the simulation conducted is relatively short compared to the time scales of natural variability, so the anthropogenic trend is not expected to be readily detectable (cf. Christian (2014); Cummins and Masson (2014)).

Biota are sensitive to the length of time over which extreme conditions occur in addition to the spatial extent and magnitude. We computed the average duration and the maximum duration of an extreme event over all of the grid cells in each cluster and then average over all of the clusters (Table 1). The average length of an event is around 1.5 days. While T and $[O_2]$ events have longer maximum duration in the Canyons, Ω_A events have longer maximum duration in the Shallows.

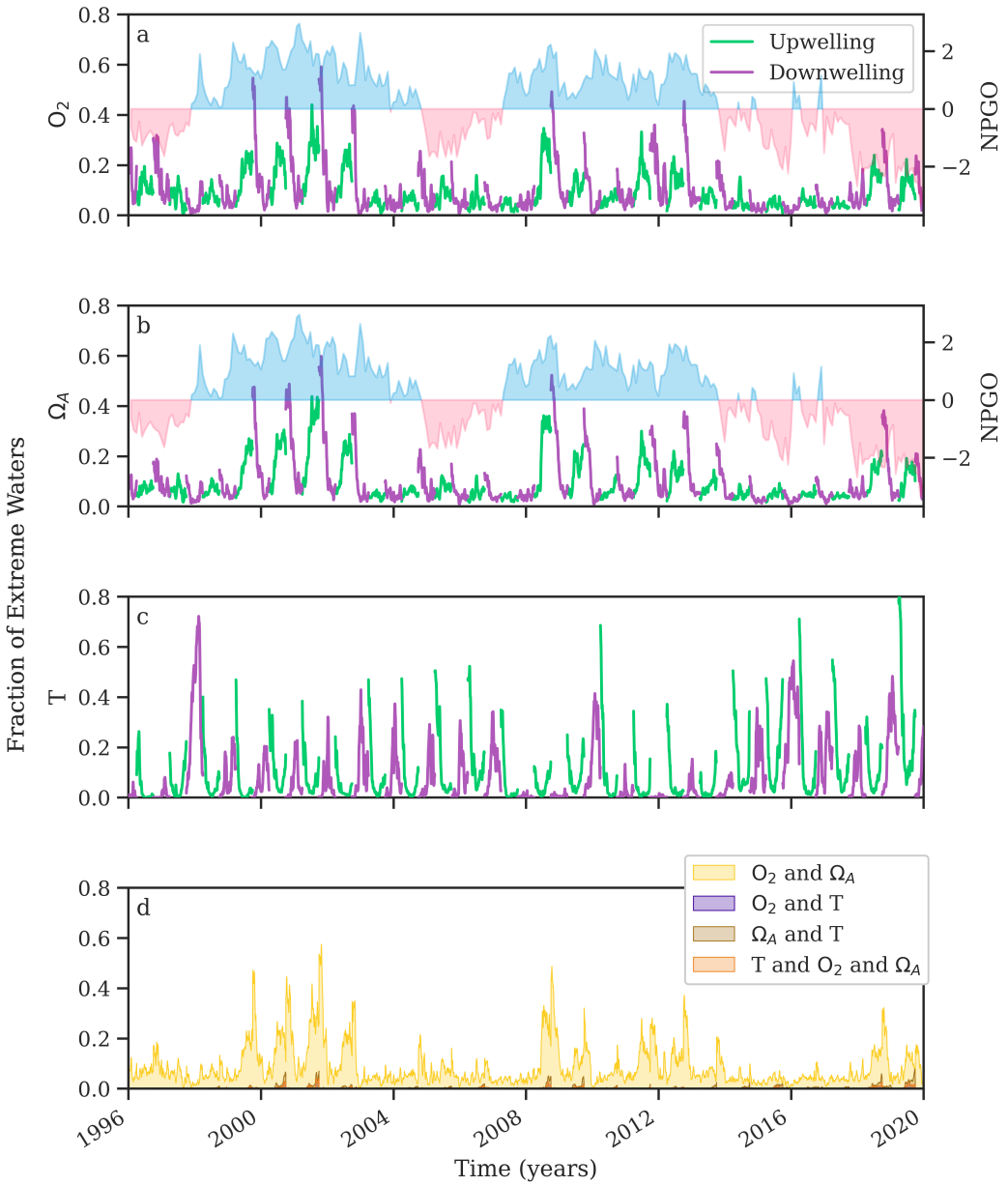

Figure 2. The fraction of waters in the Canyons that exceed the relative threshold (Table 1) for (a) dissolved oxygen, (b) aragonite saturation state, (c) potential temperature, and (d) compound stressors. The North Pacific Gyre Oscillation (NPGO) is shown on the secondary axis of (a) and (b) and is colored in red when North-Eastern Pacific waters are warm and blue when they are cold. Discontinuities at the spring and fall transition correspond to the different thresholds for each season. The compound stressors shown in panel (d) are shown individually in Figure S9.

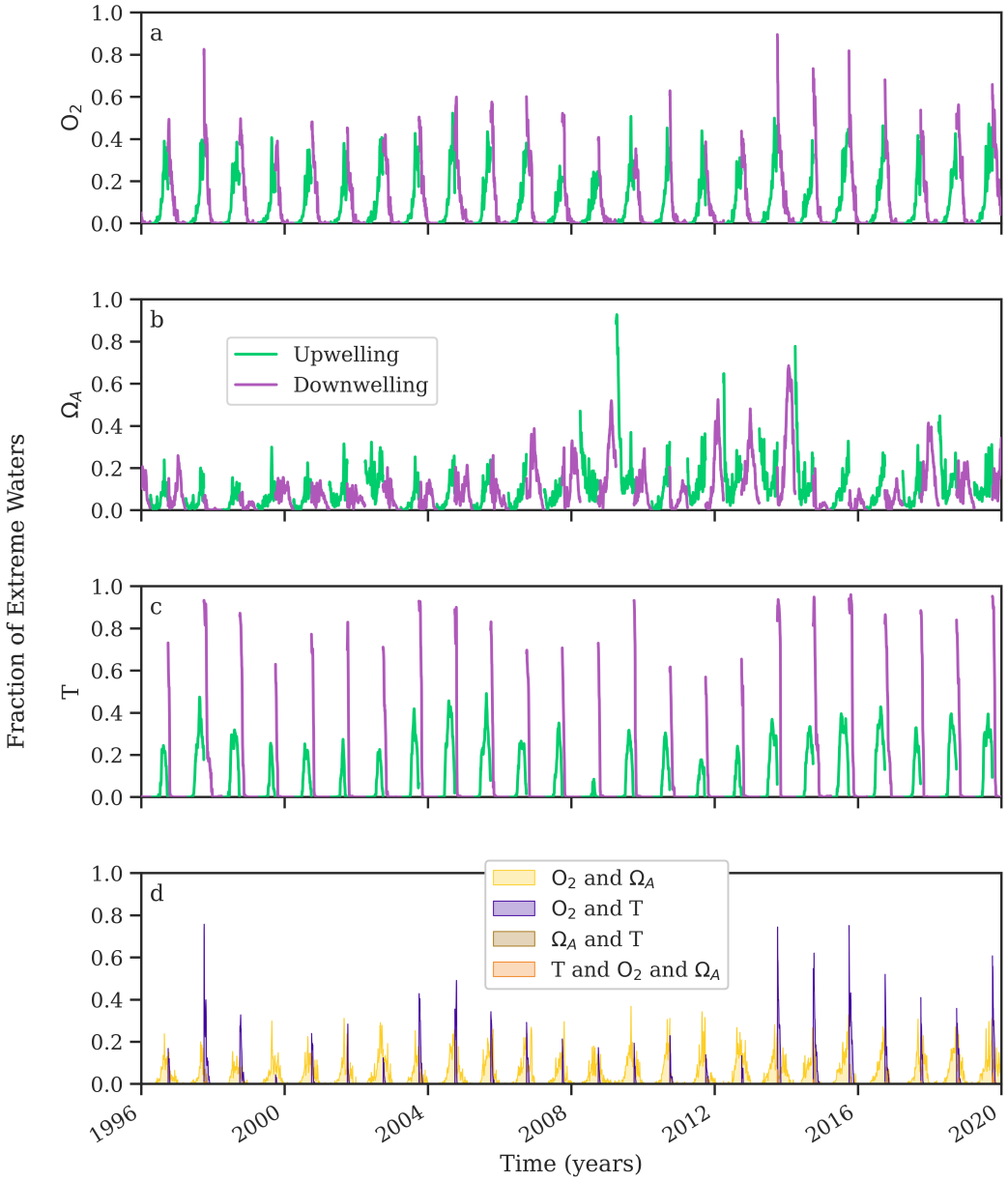

Figure 3. The fraction of waters in the Shallows that exceed the relative threshold (Table 1) for (a) dissolved oxygen, (b) aragonite saturation state, (c) potential temperature, and d) compound stressors. Discontinuities at the spring and fall transition correspond to the different thresholds for each season. The compound stressors shown in panel (d) are shown individually in Figure S10.

Compound extremes (i.e., the occurrence of extreme conditions in two or more stressors at once) can have synergistic effects on marine organisms (Pörtner et al., 2005). The Shallows frequently exhibited compound T and [O_2] extremes during the downwelling season (Figure 3d and Figure S10b). Yet, the only years for which all three stressors exceeded the thresholds in the Shallows for $> 5\%$ of waters were MHW years: 2014, the year of the anomalous warming pattern referred to as The Blob, and 2019, referred to as The Blob-2.0 (Amaya et al., 2020)(Figure 3d, Figure S10d). For the Canyons, compound extremes are relatively rare (Figure 2d and Figure S9) with the exception of [O_2] and Ω_A which exhibit the same pattern of variability as the single stressor extremes. Notably, the two periods during which we have a substantial fraction of single and compound extremes for O_2 and Ω_A in the Canyons (Figure 2 and Figure S9a) are periods during which the NPGO is positive and is associated with enhanced upwelling in the California Current system (Di Lorenzo et al., 2008).

The other four clusters show similar patterns of variability with very few triple extremes and, for most clusters, less than 5% of waters are extreme before 2014 (Figure S11). Three of the clusters ('b', 'd', 'e') exhibit a statistically significant ($p< 0.05$) trend in triple extremes (Text S3). This result is consistent with Hauri et al. (2024) who characterized extremes for the benthic regions of the shelf in the Gulf of Alaska; they found a greater fraction of waters experiencing compound (Ω_A / O_2) extremes, but the methodologies are not directly comparable. They attributed the increase in extremes at the end of the time series to the secular trends of anthropogenic warming and ocean acidification. The secular trend likely explains the increase in triple extremes for these shallower clusters where the maximum mixed layer depth (MLD) is near the ocean bottom (Text S3).

4 Discussion

We introduced a method for characterizing extreme conditions in a regional ocean model. For NEP36-CanOE, daily temporal resolution was sufficient to resolve the extremes (Text S2). While the model was highly correlated with available observations for the relevant variables (section 2.1 and Text S1), it was limited by the fact that we used climatologies for the rivers and did not include the effects of fluvial nutrients. We restricted the environmental conditions used in the unsupervised clustering approach to indices of warming, deoxygenation, and acidification. The two clusters selected for discussion are of ecological importance because of their high biodiversity (Rubidge et al., 2016) and contrasting environmental conditions (Table 1). These contrasting characteristics allow us to distinguish between different mechanistic drivers for marine extremes in the entire domain.

Thresholds defining extremes for each potential stressor were established separately for the upwelling and downwelling seasons because they represent different oceanographic regimes, and coincide with changes in the mean direction of flow of coastal currents (Thomson & Krassovski, 2010). These seasons are relevant to benthic organisms that are adapted to local conditions. Marine organisms may be in different life stages during these seasons, with different tolerance levels depending on life stage (Stachura et al., 2014; Hobday et al., 2016). For example, consider two economically important species from the Shallows and Canyons: Dungeness crab, which experience seasonal vulnerability as a result of their complex life cycle (Berger et al., 2021), and rockfish, whose juvenile abundance is linked to nearshore temperatures in February and March (Ainley et al., 1993; Laidig et al., 2007) and for which coastal downwelling has been shown to influence recruitment (Markel & Shurin, 2020).

The extreme thresholds (Table 1) in the Canyons cluster are closer to established ecological thresholds (Vaquer-Sunyer & Duarte, 2008) which makes this cluster particularly vulnerable. However, ecosystem reorganizations may develop progressively rather

than abruptly because different species have different tolerance levels (Pörtner et al., 2005). Even if the statistical thresholds are not life threatening to a particular organism, they can still have detrimental effects on growth and reproductive success if species are well adapted to their environmental conditions.

Although compound extremes are rare, they are increasing for some clusters. The Canadian northeastern Pacific region shares many ecosystem attributes and physical drivers with other eastern boundary current upwelling systems with similar future projections of warming, deoxygenation and increasing acidification (Bograd et al., 2023). Therefore, recent and potential future increases in compound extremes have global relevance because they present a threat to the ecosystem services that these systems provide.

Compound extremes can be particularly detrimental to organisms because of their synergistic effects (Pörtner, 2010) and further investigation into how these extremes could affect organisms is warranted. Our definition of extremes occurring at the same time and in the same grid cell is potentially too restrictive for mobile organisms. An approach which considers the entire water column (Wong et al., 2024) may be more appropriate for organisms that can move vertically, or laterally to different depths on the seafloor.

The upwelling and downwelling seasons impact the Shallows and Canyons differently, which can be partly attributed to their relative depths (Figure 1). The Canyons are strongly influenced by upwelling waters that are relatively cold and low in oxygen with a low Ω_A, and only weakly influenced by surface T changes. The Shallows experience much more temperature variability in response to the seasonally changing atmosphere and are only weakly influenced by upwelled waters. Consequently, the Canyons experience more frequent compound extremes in Ω_A and $[O_2]$, while the shallows experience more frequent compound extremes in $[O_2]$ and T (Figs. S9 and S10).

We hypothesize that much of the interannual variability in the percentage of waters that exceed the thresholds (Figs. 2 and 3) can be explained by the strength and length of seasonal upwelling/downwelling in the Canyons, and direct forcing by the atmosphere in the Shallows. There are many factors that contribute to the relative influence of each of these processes on extreme conditions for the cluster and season including the timing of the spring and fall transitions, mixing and stratification of the water column, changes in the California Undercurrent, and coastally trapped waves (Thomson & Krassovski, 2010; Engida et al., 2016; Mogen et al., 2022; Franco et al., 2023; Amaya et al., 2023). Because the clusters are stratified by depth, the relative contribution of upwelling from below and atmospheric forcing from above is influenced by the average depth of the cluster relative to the MLD (Text S3, Table S3).

Correlations between the single stressor extremes and the NPGO, Multivariate ENSO Index (MEI), Pacific Decadal Oscillation (PDO) and Bakun upwelling index provide evidence that changes in upwelling and downwelling and large scale atmospheric forcing drive the variability in extremes (Figure S13 and Text S4). While the only local indicator that we examined was the Bakun index, the correlations (Figure S13) support the conclusion that large scale indicators (NPGO, PDO and MEI) are more predictive of ecosystem change along the continental margin than local indicators (Hallett et al., 2004; Li et al., 2013; Mackas et al., 2013).

5 Conclusions

Characterizing the occurrence of extremes in the recent past when they occur in isolation, or in combination is a step towards understanding the risks that they pose to local ecosystems and fisheries. This study presented a simple approach for statistically characterizing extreme marine conditions of high temperature, low oxygen, and high acidification. We applied it to a numerical model of the Northeastern Pacific continental margin, but it can be adapted to other regions and time periods. We used unsupervised clus-

tering to isolate regions with similar environmental conditions and defined the extremes using a relative threshold with a fixed baseline (1996-2020) (Hobday et al., 2016; Gruber et al., 2021).

The analysis of extremes in the Northeastern Pacific demonstrated that the strength of seasonal upwelling/downwelling and direct forcing by the atmosphere strongly influence extreme conditions. Large scale processes (like the NPGO) may be more predictive of extreme conditions of $[O_2]$ and Ω_A than local indicators like the Bakun index and further investigation of these relationships is needed. While a substantial number of single stressor extremes occur annually, compound extremes are rare. Most of the multiple stressor extremes involve coincident O_2 and Ω_A extremes, with a greater number in the Canyons than the Shallows. Multiple stressor extremes are increasing for clusters where the mixed layer extends to near the ocean bottom. Under future climate change, compound extremes may become more common, with detrimental effects on ecologically and commercially important species.

6 Open Research

The open source code that the ocean model is based on here `https://www.nemo-ocean.eu/` The observational data used to evaluate the model is available online including the ship-sampled data (Department of Fisheries and Oceans Canada (DFO), 2022), tide gauge data (NRCan, 2022) and mixed layer depths (NOAA Pacific Marine Environmental Laboratory, 2021). The model data needed for the analysis can be found here `https://doi.org/10.5281/zenodo.13138494` (Holdsworth et al., 2024a). The python notebooks used for the analysis of the data is found on Github here `https://github.com/ashao/NEP36_cluster_analysis` (Holdsworth et al., 2024b) and will be added to a zenodo repository for permanent storage if this manuscript is published.

Acknowledgments
Special thanks to Lu Guan for her assistance with in situ data and to Michael Dunphy and colleagues working on the Oceans Protection Plan for use of their evaluation toolset. Thanks to Tetjana Ross and Emily Rubidge for useful comments on an earlier draft, and Cathy Reader, Tessa Sou, and Nadja Steiner for useful discussions about this work. Thanks to all of the contributors to the datasets used for this study including GLODAP (Key et al., 2015; Lauvset et al., 2016), ERA5 (Hersbach et al., 2018), GLORYS12 (Lellouche et al., 2021), WOA (Garcia et al., 2019a, 2019b), NOAA's climate indices (Di Lorenzo, 2022; NOAA Physical Sciences Laboratory, 2022; NOAA Pacific Fisheries Environmental Laboratory, 2022; NOAA Physical Sciences Laboratory, 2024), and the observations used for evaluation (NOAA Pacific Marine Environmental Laboratory, 2021; Schmidtko et al., 2013; Department of Fisheries and Oceans Canada (DFO), 2022; NRCan, 2022).

References

Ainley, D. G., Sydeman, W., Parrish, R., & Lenarz, W. (1993). Oceanic factors influencing distribution of young rockfish (*Sebastes*) in central California: a predator's perspective. *California Cooperative Oceanic Fisheries Investigations Reports*, *34*, 133–139.

Amaya, D. J., Jacox, M. G., Alexander, M. A., Scott, J. D., Deser, C., Capotondi, A., & Phillips, A. S. (2023). Bottom marine heatwaves along the continental shelves of North America. *Nature Communications*, *14*(1), 1038. doi: DOI={10.1038/s41467-023-36567-0}

Amaya, D. J., Miller, A. J., Xie, S.-P., & Kosaka, Y. (2020). Physical drivers of the summer 2019 North Pacific marine heatwave. *Nature Communications*, *11*(1903). doi: 10.1038/s41467-020-15820-w

Berger, H. M., Siedlecki, S. A., Matassa, C. M., Alin, S. R., Kaplan, I. C., Hodgson, E. E., ... Newton, J. A. (2021). Seasonality and life history complexity determine vulnerability of Dungeness crab to multiple climate stressors. *AGU Advances*, *2*(4). doi: 10.1029/2021AV000456

Bograd, S. J., Jacox, M. G., Hazen, E. L., Lovecchio, E., Montes, I., Buil, M. P., ... Rykaczewski, R. R. (2023). Climate change impacts on eastern boundary upwelling systems. *ANNUAL REVIEW OF MARINE SCIENCE*, *15*, 303-328. doi: 10.1146/annurev-marine-032122-021945

Boldt, J. L., Chandler, P. C., & King, S. A. (2020). State of the physical, biological and selected fishery resources of Pacific Canadian marine ecosystems in 2019. *Canadian Technical Report of Fisheries and Aquatic Sciences*, *3266*.

Breitburg, D., Levin, L. A., Oschlies, A., Grégoire, M., Chavez, F. P., Conley, D. J., ... Zhang, J. (2018). Declining oxygen in the global ocean and coastal waters. *Science*, *359*(6371), eaam7240. doi: 10.1126/science.aam7240

Cavole, L. M., Demko, A. M., Diner, R. E., Giddings, A., Koester, I., Pagniello, C., ... Franks, P. J. S. (2016). Biological impacts of the 2013–2015 warm-water anomaly in the northeast Pacific: Winners, losers, and the future. *Oceanography*, *29*(2), 273-285. doi: 10.5670/oceanog.2016.32

Cheung, W. W., & Frölicher, T. L. (2020). Marine heatwaves exacerbate climate change impacts for fisheries in the northeast Pacific. *Scientific Reports*, *10*(6678). doi: 10.1038/s41598-020-63650-z

Christian, J. R. (2014). Timing of the departure of ocean biogeochemical cycles from the preindustrial state. *PLoS One*, *9*(11), e109820. doi: 10.1371/journal.pone.0109820

Christian, J. R., Denman, K. L., Hayashida, H., Holdsworth, A. M., Lee, W. G., Riche, O. G., ... Swart, N. C. (2022). Ocean biogeochemistry in the Canadian Earth system model version 5.0.3: CanESM5 and CanESM5-CanOE. *Geoscientific Model Development*, *15*(11), 4393–4424. doi: 10.5194/gmd-15-4393-2022

Cummins, P. F., & Masson, D. (2014). Climatic variability and trends in the surface waters of coastal British Columbia. *Progress in Oceanography*, *120*, 279–290.

Cushing, D. (1971). Upwelling and the production of fish. In *Advances in marine biology* (Vol. 9, pp. 255–334). Elsevier. doi: 10.1016/s0065-2881(08)60344-2

Department of Fisheries and Oceans Canada (DFO). (2022). *Institute of Ocean Sciences Data Archive* [Data set]. (Data obtained on 2022/05/15 from `www.waterproperties.ca`)

Di Lorenzo, E. (2022). *The North Pacific Gyre Oscillation (NPGO)* [Data set]. (Data obtained on 11/25/2022 from `https://www.o3d.org/npgo/data/NPGO.txt`)

Di Lorenzo, E., Schneider, N., Cobb, K. M., Franks, P. J. S., Chhak, K. C., Miller, A. J., ... Rivière, P. (2008). North Pacific Gyre Oscillation links ocean climate and ecosystem change. *Geophysical Research Letters*, *35*(8). doi: 10.1029/2007GL032838

Engida, Z., Monahan, A., Ianson, D., & Thomson, R. E. (2016). Remote forcing of subsurface currents and temperatures near the northern limit of the California Current system. *Journal of Geophysical Research: Oceans*, *121*(10), 7244–7262. doi: 10.1002/2016JC011880

Franco, A. C., Ianson, D., Ross, T., Hannah, C., Sastri, A., & Tortell, P. D. (2023). Drivers and potential consequences of observed extreme hypoxia along the Canadian Pacific continental shelf. *Geophysical Research Letters*, *50*(6), e2022GL101857. doi: 10.1029/2022GL101857

Frölicher, T. L., Fischer, E. M., & Gruber, N. (2018). Marine heatwaves under global warming. *Nature*, *560*(7718), 360–364. doi: 10.1038/s41586-018-0383-9

Garcia, H., Weathers, K., Paver, C., Smolyar, I., Boyer, T., Locarnini, M., ... Seidov, D. (2019a). *World Ocean Atlas 2018. vol. 4: Dissolved inorganic nutrients*

(phosphate, nitrate and nitrate+ nitrite, silicate).

Garcia, H., Weathers, K., Paver, C., Smolyar, I., Boyer, T., Locarnini, M., ... Seidov, D. (2019b). *World Ocean Atlas 2018, volume 3: Dissolved oxygen, apparent oxygen utilization, and dissolved oxygen saturation.*

Gruber, N. (2011). Warming up, turning sour, losing breath: ocean biogeochemistry under global change. *Philosophical Transactions of the Royal Society A: Mathematical, Physical and Engineering Sciences*, *369*(1943), 1980–1996. doi: 10.1098/rsta.2011.0003

Gruber, N., Boyd, P. W., Frölicher, T. L., & Vogt, M. (2021). Biogeochemical extremes and compound events in the ocean. *Nature*, *600*(7889), 395–407. doi: 10.1038/s41586-021-03981-7

Hallett, T., Coulson, T., Pilkington, J., Clutton-Brock, T., Pemberton, J., & Grenfell, B. (2004). Why large-scale climate indices seem to predict ecological processes better than local weather. *Nature*, *430*(6995), 71–75. doi: 10.1038/nature02708

Hauri, C., Pages, R., Hedstrom, K., Doney, S. C., Dupont, S., Ferriss, B., & Stuecker, M. F. (2024). More than marine heatwaves: A new regime of heat, acidity, and low oxygen compound extreme events in the Gulf of Alaska. *AGU Advances*, *5*(1), e2023AV001039. doi: 10.1029/2023AV001039

Hersbach, H., Bell, B., Berrisford, P., Biavati, G., Horányi, A., Muñoz Sabater, J., ... Schepers, D. (2018). ERA5 hourly data on single levels from 1979 to present. *Copernicus Climate Change Service (C3S) Climate Data Store (CDS)*, *10*. (Accessed on 06-06-2021) doi: 10.24381/cds.adbb2d47

Hobday, A. J., Alexander, L. V., Perkins, S. E., Smale, D. A., Straub, S. C., Oliver, E. C., ... Wernberg, T. (2016). A hierarchical approach to defining marine heatwaves. *Progress in Oceanography*, *141*, 227–238. doi: 10.1016/j.pocean.2015.12.014

Holdsworth, A. M., Shao, A., & Christian, J. R. (2024a). *Data used to produce the results for the article "clustering to characterize extreme marine conditions for the benthic region of northeastern pacific continental margin"* [Data set]. Zenodo. doi: 10.5281/zenodo.13138494

Holdsworth, A. M., Shao, A., & Christian, J. R. (2024b). *Notebooks used to produce the results for the article "clustering to characterize extreme marine conditions for the benthic region of northeastern pacific continental margin"* [ComputationalNotebook]. GitHub. (`https://github.com/ashao/NEP36_cluster_analysis`)

Holdsworth, A. M., Zhai, L., Lu, Y., & Christian, J. R. (2021). Future changes in oceanography and biogeochemistry along the Canadian Pacific continental margin. *Frontiers in Marine Science*, *8*. doi: 10.3389/fmars.2021.602991

Hurd, C. L., Beardall, J., Comeau, S., Cornwall, C. E., Havenhand, J. N., Munday, P. L., ... McGraw, C. M. (2019). Ocean acidification as a multiple driver: how interactions between changing seawater carbonate parameters affect marine life. *Marine and Freshwater Research*, *71*(3), 263–274. doi: 10.1071/MF19267

Jackson, E. K., Roberts, W., Nelsen, B., Williams, G. P., Nelson, E. J., & Ames, D. P. (2019). Introductory overview: Error metrics for hydrologic modelling–a review of common practices and an open source library to facilitate use and adoption. *Environmental Modelling & Software*, *119*, 32–48. doi: 10.1016/j.envsoft.2019.05.001

Keeling, R. F., Körtzinger, A., & Gruber, N. (2010). Ocean deoxygenation in a warming world. *Annual Review of Marine Science*, *2*(1), 199–229. doi: 10.1146/annurev.marine.010908.163855

Key, R. M., Olsen, A., van Heuven, S., Lauvset, S. K., Velo, A., Lin, X., ... Jutterström, S. (2015). Global Ocean Data Analysis Project, version 2 (GLODAPv2). *ORNL/CDIAC-162, NDP-093*.

Kling, H., Fuchs, M., & Paulin, M. (2012). Runoff conditions in the upper Danube

basin under an ensemble of climate change scenarios. *Journal of Hydrology*, *424-425*, 264-277. doi: 10.1016/j.jhydrol.2012.01.011

Kwiatkowski, L., Torres, O., Bopp, L., Aumont, O., Chamberlain, M. A., Christian, J. R., ... Ziehn, T. (2020). Twenty-first century ocean warming, acidification, deoxygenation, and upper-ocean nutrient and primary production decline from CMIP6 model projections. *Biogeosciences*, *17*(13), 3439–3470. doi: 10.5194/bg-17-3439-2020

Laidig, T. E., Chess, J. R., & Howard, D. F. (2007). Relationship between abundance of juvenile rockfishes (*Sebastes spp.*) and environmental variables documented off northern California and potential mechanisms for the covariation. *Fishery Bulletin*, *105*(1), 39–49.

Lauvset, S. K., Key, R. M., Olsen, A., van Heuven, S., Velo, A., Lin, X., ... Watelet, S. (2016). A new global interior ocean mapped climatology: The 1° × 1° GLODAP version 2. *Earth System Science Data*, *8*(2), 325–340. doi: 10.5194/essd-8-325-2016

Lellouche, J.-M., Greiner, E., Bourdallé-Badie, R., Garric, G., Melet, A., Drévillon, M., ... Le Traon, P.-Y. (2021). The Copernicus Global 1/12° Oceanic and Sea Ice GLORYS12 Reanalysis. *Frontiers in Earth Science*, *9*. doi: 10.3389/feart.2021.698876

Li, L., Mackas, D., Hunt, B., Schweigert, J., Pakhomov, E., Perry, R. I., ... Pitcher, T. J. (2013). Zooplankton communities in the Strait of Georgia, British Columbia, track large-scale climate forcing over the Pacific Ocean. *Progress in Oceanography*, *115*, 90–102. doi: 10.1016/j.pocean.2013.05.025

Mackas, D., Galbraith, M., Faust, D., Masson, D., Young, K., Shaw, W., ... Sastri, A. (2013). Zooplankton time series from the Strait of Georgia: Results from year-round sampling at deep water locations, 1990–2010. *Progress in Oceanography*, *115*, 129–159. doi: 10.1016/j.pocean.2013.05.019

Markel, R. W., & Shurin, J. B. (2020). Contrasting effects of coastal upwelling on growth and recruitment of nearshore Pacific rockfishes (genus *Sebastes*). *Canadian Journal of Fisheries and Aquatic Sciences*, *77*(6), 950–962. doi: 10.1139/cjfas-2019-0179

May, R. M., Arms, S. C., Marsh, P., Bruning, E., Leeman, J. R., Goebbert, K., ... Bruick, Z. S. (2021). *Metpy: A Python package for meteorological data.* Retrieved from `https://github.com/Unidata/MetPy` doi: 10.5065/D6WW7G29

Mogen, S. C., Lovenduski, N. S., Dallmann, A. R., Gregor, L., Sutton, A. J., & Bograd, S. J. (2022). Ocean biogeochemical signatures of the North Pacific Blob. *Geophysical Research Letters*, *49*(9), e2021GL096938. doi: 10.1029/2021GL096938

NOAA Pacific Fisheries Environmental Laboratory. (2022). *Traditional 3 degree Bakun index* [Data set]. National Oceanic and Atmospheric Administration. (Data obtained on 03/10/2022 from `oceanwatch.pfeg.noaa.gov/products/PFELData/upwell/monthly/upindex.mon`)

NOAA Pacific Marine Environmental Laboratory. (2021). *Monthly Isopycnal & Mixed-layer Ocean Climatology (MIMOC)* [Data set]. National Oceanic and Atmospheric Administration. (Data obtained on 09/15/2021 from `https://www.pmel.noaa.gov/mimoc/`)

NOAA Physical Sciences Laboratory. (2022). *The Pacific Decadel Oscillation (PDO)* [Data set]. National Oceanic and Atmospheric Administration. (Data obtained on 12/16/2022 from `https://psl.noaa.gov/pdo/`)

NOAA Physical Sciences Laboratory. (2024). *Multivariate ENSO Index Version 2 (MEI.v2)* [Data set]. National Oceanic and Atmospheric Administration. (Data obtained on 01/11/2024 from `https://www.psl.noaa.gov/enso/mei`)

NRCan. (2022). *Geodetic reference systems* [Data set]. Natural Resources Canada. (`https://www.nrcan.gc.ca/maps-tools-and-publications/tools/`

geodetic-reference-systems/canadian-spatial-reference-system-csrs/9052#cgvd28)

Pedregosa, F., Varoquaux, G., Gramfort, A., Michel, V., Thirion, B., Grisel, O., ... Duchesnay, E. (2011). Scikit-learn: Machine learning in Python [Software]. *Journal of Machine Learning Research*, *12*, 2825–2830.

Pörtner, H.-O. (2010). Oxygen-and capacity-limitation of thermal tolerance: a matrix for integrating climate-related stressor effects in marine ecosystems. *Journal of Experimental Biology*, *213*(6), 881–893. doi: 10.1242/jeb.037523

Pörtner, H. O., & Farrell, A. P. (2008). Physiology and climate change. *Science*, *322*(5902), 690–692. doi: 10.1126/science.1163156

Pörtner, H. O., Langenbuch, M., & Michaelidis, B. (2005). Synergistic effects of temperature extremes, hypoxia, and increases in CO_2 on marine animals: From Earth history to global change. *Journal of Geophysical Research: Oceans*, *110*(C9). doi: 10.1029/2004JC002561

Pörtner, H.-O., Roberts, D. C., Masson-Delmotte, V., Zhai, P., Tignor, M., Poloczanska, E., & Weyer, N. (2019). The ocean and cryosphere in a changing climate. *IPCC special report on the ocean and cryosphere in a changing climate*, *1155*. doi: 10.1017/9781009157964

Rubidge, E. M., Gale, K. S., & Curtis, J. M. (2016). Community ecological modelling as an alternative to physiographic classifications for marine conservation planning. *Biodiversity and conservation*, *25*, 1899–1920. doi: 10.1007/s10531-016-1167-x

Schmidtko, S., Johnson, G. C., & Lyman, J. M. (2013). MIMOC: A global monthly isopycnal upper-ocean climatology with mixed layers. *Journal of Geophysical Research: Oceans*, *118*(4), 1658–1672. doi: 10.1002/jgrc.20122

Smale, D. A., Wernberg, T., Oliver, E. C. J., Thomsen, M. S., Harvey, B. P., Straub, S. C., ... Moore, P. J. (2019). Marine heatwaves threaten global biodiversity and the provision of ecosystem services. *Nature Climate Change*, *9*(4), 306–312. doi: 10.1038/s41558-019-0412-1

Stachura, M. M., Essington, T. E., Mantua, N. J., Hollowed, A. B., Haltuch, M. A., Spencer, P. D., ... Doyle, M. J. (2014). Linking Northeast Pacific recruitment synchrony to environmental variability. *Fisheries Oceanography*, *23*(5), 389–408. doi: 10.1111/fog.12066

Thompson, P. L., Anderson, S. C., Nephin, J., Robb, C. K., Proudfoot, B., Park, A. E., ... Rubidge, E. M. (2022). Integrating trawl and longline surveys across British Columbia improves groundfish distribution predictions. *Canadian Journal of Fisheries and Aquatic Sciences*, *80*(1), 195–210. doi: 10.1139/cjfas-2022-0108

Thompson, P. L., Nephin, J., Davies, S. C., Park, A. E., Lyons, D. A., Rooper, C. N., ... Holdsworth, A. M. (2023). Groundfish biodiversity change in northeastern Pacific waters under projected warming and deoxygenation. *Philosophical Transactions of the Royal Society B: Biological Sciences*, *378*(1881), 20220191. doi: 10.1098/rstb.2022.0191

Thomson, R. E., & Krassovski, M. V. (2010). Poleward reach of the California Undercurrent extension. *Journal of Geophysical Research: Oceans*, *115*(C9). doi: 10.1029/2010JC006280

Vaquer-Sunyer, R., & Duarte, C. M. (2008). Thresholds of hypoxia for marine biodiversity. *Proceedings of the National Academy of Sciences*, *105*(40), 15452–15457. doi: 10.1073/pnas.0803833105

von Biela, V. R., Arimitsu, M. L., Piatt, J. F., Heflin, B., Schoen, S. K., Trowbridge, J. L., & Clawson, C. M. (2019). Extreme reduction in nutritional value of a key forage fish during the Pacific marine heatwave of 2014-2016. *Marine Ecology Progress Series*, *613*, 171–182. doi: 10.3354/meps12891

Wong, J., Münnich, M., & Gruber, N. (2024). Column-compound extremes in the global ocean. *AGU Advances*, *5*(3), e2023AV001059. doi: 10.1029/

2023AV001059

Zacharias, M. A., Howes, D. E., Harper, J. R., & Wainwright, P. (1998). The British Columbia marine ecosystem classification: rationale, development, and verification. *Coastal Management*, *26*(2), 105–124. doi: 10.1080/08920759809362347

Supporting Information for "Clustering to characterize extreme marine conditions for the benthic region of Northeastern Pacific continental margin"

Amber M. Holdsworth[1], Andrew Shao[2], and James R. Christian[13]

[1]Fisheries and Oceans Canada

[2]Hewlett Packard Enterprise

[3]Canadian Centre for Climate Modelling and Analysis

Contents of this file

1. Text S1 to S4
2. Figures S1 to S13
3. Tables S1 to S3

Introduction

The supporting information consists of additional details about model and methods used, and additional evidence for results presented in the main text. Text S1 provides additional details of regional model development and evaluation with observations (Figures S1-S5, Tables S1 and S2). Text S2 provides additional information on the cluster

analysis and computed thresholds (Figures S6-S8, Table S3). Text S3 provides supporting information on the compound extremes (Figures S9-S11) and event durations. Finally, Text S4 provides details of the climate indices and correlation analysis (Figures S12 and S13).

Text S1: North-Eastern Pacific Canadian Ocean Ecosystem Model

This section will detail recent improvements to the model including the addition of a new module for benthic remineralization, tuning of the community structure in CanOE and evaluation of the model.

The regional ocean model, NEP36-CanOE, is an updated version of the one used in Holdsworth, Zhai, Lu, and Christian (2021),with 75 vertical levels instead of 50, a time step of 180 s instead of 60 s (except in the vertical), improved model bathymetry, tidal loading and attraction from Lyard, Allain, Cancet, Carrère, and Picot (2021), and the TKE scheme for vertical mixing. The biogeochemical model uses 19 tracers and each phytoplankton group has four state variables: nitrogen, carbon, iron, and chlorophyll. We have turned off iron limitation.

The model has a large computational domain with $714 \times 1020 \times 75 = 54\,621\,000$ points. To reduce the amount of data stored on disk, we output monthly averages for the entire model and daily averages for the continental shelf (Figure S1). Only the daily averages are used for this study, and the domain is reduced to exclude open ocean regions more than 55 grid cells (> 100 km) seaward of the 500 m isobath (in the x-direction). Regions where the model is not expected to perform well due to limited resolution are excluded from our analysis of extremes (Fig. S1).

We ran a perpetual cycle of the year 1996 until the model reached equilibrium (nearly repeating annual cycle). This process took 6 years for the physics and an additional 4 years with biogeochemistry turned on.

Benthic remineralization parameterization

Organic matter produced in the euphotic zone sinks through the water column. Some of it is remineralized as it sinks, and some of it is deposited on the seafloor where it is respired or buried in the sediments. Larger organisms such as clams and worms in the sediment carry out aerobic respiration, while bacteria are capable of remineralization even in the absence of oxygen (Sarmiento & Gruber, 2006). The timing, amount and freshness of the organic deposition have important consequences for the structure of benthic communities (Soetaert et al., 2000; Heip et al., 2001) and affect the timing and magnitude of sedimentary nutrient efflux and oxygen demand.

This section details the integrated sediment model that we implemented in the Canadian Ocean Ecosystem model (CanOE). The simple parameterization for the sediments that was already implemented in CanOE is known as a reflective boundary. All particulate materials deposited on the sea-floor are instantaneously transformed into nutrients and inorganic carbon in the deepest ocean layer (Soetaert et al., 2000). While the existing parameterization conserves mass and is computationally efficient, it is not particularly realistic. Bianucci, Denman, and Ianson (2011) considered these models as well as a resuspension experiment in which the organic matter reaching the seafloor remains in the lower grid cell of the water column as detritus. They found that for West Coast Vancouver Island the "resuspension" parameterization may be most appropriate because

it is a highly energetic environment (Bianucci et al., 2011). However, this region is only a small fraction of the NEP36 domain, and other regions have much less near-bottom shear and turbulence. A full diagenetic model would be computationally expensive and there is evidence that the model derived denitrification rates are significantly smaller than the true rates measured in situ (Devol, 1991). Therefore, we implemented an idealized vertically integrated model with a single sediment layer and a specified, constant fraction of remineralization as denitrification.

There are no direct measurements of sediment fluxes for the Canadian Pacific Ocean. Along the Washington State continental margin Devol (1991) and Devol and Christensen (1993) measured the benthic fluxes of O_2, NH_4, NO_3, N_2, $Si(OH)_4$ and PO_4. These are the only direct measurements of denitrification (N_2 flux) globally and relatively few shelf and slope areas have been studied (Seitzinger & Giblin, 1996).

The idealized model is conceptualized as an infinitesimally thin (essentially 2D) active layer. Organic matter deposited on the seafloor is remineralized, exchanging $[O_2]$ and DIC with the water column. All of the organic nitrogen arriving at the seafloor is transformed to NH_4 within the sediments by microorganisms in a process known as ammonification, and we assume that all of the NH_4 is consumed during nitrification which demands an additional flux of $[O_2]$ from the water column to produce NO_3. Denitrification within the sediment layer consumes all of the NO_3 generated via nitrification, and the remaining demand for nitrate is supplied from the ocean model grid cell at the ocean bottom. The denitrification fraction of remineralization is fixed at 28% Devol (1991).

CanOE includes two different pools for particulate organic carbon (nitrogen): POC (PON) for the smaller class ($1 - 100\mu\,\mathrm{m}$) with a sinking rate $\omega_P = 2\,\mathrm{m\,d^{-1}}$ and GOC (GON) for the larger class ($100 - 5000\mu\,\mathrm{m}$) with a sinking rate $\omega_G = 30\,\mathrm{m\,d^{-1}}$ and the deposition of organic carbon to the seafloor is defined by $\mathrm{deposition}_C = \omega_P \mathrm{POC}|_{z=h} + \omega_G \mathrm{GOC}|_{z=h}$. Organic matter in the sediment is oxidized at a rate $r_{sedC}\,(\mathrm{d^{-1}})$ which gives $\mathrm{remin}_C = F_{DIC} = r_{sedC} C_{sed}$. Here we are assuming that remineralization (aerobic) and denitrification (anaerobic) produce the same amount of DIC (Fennel et al., 2006; Bianucci et al., 2011). The model has a single sediment pool for carbon C_{sed} from which nitrogen and iron are implicitly derived according to specified stoichiometric relationships. The change in the carbon sediment mass $C_{sed}\,(\mathrm{mmol\,m^{-3}})$ is represented by

$$\frac{dC_{sed}}{dt} = (\mathrm{deposition}_C - \mathrm{remin}_C). \tag{1}$$

CanOE does not assume fixed elemental ratios for phytoplankton, but it does for zooplankton and detritus; as only detritus is deposited to the sea floor, we assume Redfield stoichiometry (Redfield, 1963) for remineralization. We are assuming that remineralization is divided between aerobic and denitrification; other electron acceptors like Mn or $\mathrm{SO_4^{2-}}$ are assumed to be of negligible importance on the time scales considered. Although the supply of oxygen is unlikely to be limiting, this case is dealt with in the model by turning off remineralization ($F_{DIC} = 0$) when there is an insufficient supply of oxygen. For simplicity, we do not allow for denitrification to occur in the absence of aerobic mineralization. We use a reflective boundary for iron, as iron is assumed to not be limiting in this environment.

We assume that the fraction of the remineralization due to denitrification is $\gamma = 28\%$ based on Devol (1991). In the water column, CanOE assumes that a fraction of denitrification occurs via anaerobic ammonium oxidation (anammox) (Christian et al., 2022), but we do not consider anammox in the sediments. Using a balanced equation for denitrification, we define the fluxes of nitrogen and oxygen due to remineralization as

$$F_{NO_3} = -F_{DIC}(\Phi\gamma - R_{N:C}) \tag{2}$$

$$F_{O_2} = -F_{DIC}(1-\gamma) - 2R_{N:C}F_{DIC} \tag{3}$$

where $R_{C:O} = 1$ and $R_{N:C} = 16/106$ are the Redfield ratios

There are also sources and sinks of alkalinity (TAlk) associated with remineralization and nitrification, a gain (1 mol TAlk / mol N) from remineralization and a loss (-2 mol TAlk / mol N) from nitrification, for a net of -1 assuming complete oxidation of all organic nitrogen to NO_3 (Wolf-Gladrow et al., 2007).

$$F_{TAlk} = -R_{N:C}F_{DIC} + \gamma\Phi F_{DIC}. \tag{4}$$

For this domain, the parameterization did not make an appreciable difference in the representation of O_2 or NO_3 and only marginally improved the representation of DIC and TAlk.

Tuning of biology parameters for the Northeastern Pacific continental margin

The biogeochemistry model, CanOE, was originally tuned for the global ocean. The model is computationally expensive to run so a series of 6 month sensitivity tests were used to adjust the model towards the observed total chlorophyll (Department of Fisheries and Oceans Canada (DFO), 2022). We used the following criterion based on empirical

evidence in the literature: 1. Based on a wet weight of 250 (c.f. Figure 4 of Denman and Pena (2002)), peak values of mesozooplankton are expected to be around 1.4 mmol C m^{-3}, and 2. the amount of chlorophyll in diatoms should be at least 4 times greater than in nanophytoplankton for high concentrations of phytoplankton (c.f. Chisholm (1992) Figure 9).

Using 1939 ship-sampled observations of the total chlorophyll, we evaluated the model's ability to simulate productivity before (Figure S2a) and after (Fig. S2b and c) the tuning exercise. While the model and observations are only weakly correlated (Table S2), the model is now able to represent much larger values of TChl which is more appropriate for this highly productive region.

Model evaluation

The model was evaluated against available ship-sampled observations including 263 605 T and S data, 39 067 [O_2], 5 894 [NO_3], 177 [TAlk] and 237 [DIC] (Department of Fisheries and Oceans Canada (DFO), 2022). Several evaluation metrics were computed using the HydroErr toolbox (Roberts et al., 2018); the coefficient of determination (unitless), the root mean squared error signed by the bias (data units), and the Kling-Gupta decomposition (dimensionless) (Kling et al., 2012). The decomposition consists of the Pearson score r which measures the correlation, the flow variability which is a ratio of the standard deviations $\alpha = \sigma_{\text{mod}}/\sigma_{\text{obs}}$, the bias ratio which is a ratio of the means $\alpha = \mu_{\text{mod}}/\mu_{\text{obs}}$ (Table S2). Values near 1 are optimal for these terms and they can be summarized using a single number known as the Kling-Gupta Efficiency (KGE). Values of KGE > -0.41 mean that the model is outperforming the mean flow benchmark (Knoben et al., 2019).

The model performs better than the mean flow benchmark for all data fields and, with the exception of the total chlorophyll, all KGE efficiencies are near 1 (Table S2).

The probability density functions show that the distributions of these variables are well represented by the model (Figure S3). To evaluate how well the model represents extreme conditions, we estimated the 90^{th} and 10^{th} percentiles using the distributions shown in Figure S3 and (Fig. S2c). The highest concentrations of O_2 and TChl are not reproduced by the model. However, the focus of this study is on the lowest values, and this shows that the extremes found in the observations are well represented by the model (Table S2).

The Monthly Isopycnal / Mixed-layer Ocean Climatology (MIMOC) (Schmidtko et al., 2013) was used to evaluate the mixed layer depth (MLD) and, for consistency, the Holte and Talley (2009) algorithm was used to calculate the MLD. A series of locations along the 500 m isobath of the continental shelf were used for comparison with the monthly climatologies. We found a RMSE of 10.4 m, a KGE of 0.76, and $R^2 = 0.92$. The largest discrepancies occur during winter months when MLDs are deepest (Figure S4).

Tide gauge observations from 65 different stations were transformed from the Canadian Hydrographic Service (CHS) chart datum to CGDV28 (NRCan, 2022) using station specific offsets provided by CHS using their 2015 dynamic topography model. The analysis was conducted for each year, then averaged to obtain a measure for each individual station. Note that data is missing for some stations for some of the years. The average Root Mean Squared Error (RMSE) over all of the stations is 0.33 ± 0.17 m ranging from 0.79 m to 0.11 m with $R^2 = 0.95$ (Fig. S5). The performance of the tides varies spatially with

higher RMSE within the Salish Sea where the resolution may not be adequate to resolve bathymetric features.

The tidal amplitude and phase were computed for several of the tidal constituents to evaluate the model performance. The mean of the bias (model-obs) was found for each of the stations, then the average magnitude and standard deviation were computed resulting in a single value reported in Table S1. We also compute the tidal error; the RMS difference over a tidal cycle between the model and observations (Cummins and Oey (1997), eq. 3).

Ocean acidification

We derive the aragonite saturation state, Ω_A using the pyco2sys python package (Humphreys et al., 2022), and use it as a measure of the ocean acidification as it is a biologically relevant quantity. The saturation state of seawater with respect to $CaCO_3$ is $\Omega_A = \frac{[\mathrm{Ca}^{+}][\mathrm{CO}_3^{2-}]}{\mathrm{k}_{sp}}$ where k_{sp} is the apparent solubility product for aragonite, a distinct crystalline form of $CaCO_3$. When $\Omega_A < 1$ the water is undersaturated which is conducive to shell dissolution. Model T and S are used to calculate k_{sp} and $[\mathrm{Ca}^{3+}]$ and $[\mathrm{CO}_3^{2-}]$ are calculated from modeled T, S, DIC and TAlk using pyco2sys.

Text S2: Clusters and thresholds

The prevailing surface circulation west of British Columbia's continental shelf naturally divides the region into Northern and Southern regions as the Subarctic current diverges into two distinct branches; the Alaska Current flows northeast into the Gulf of Alaska and the California Current curves to the Southeast (Thomson, 1981). The bifurcation of the current occurs between 45° and 50°N, but varies seasonally so that the division is largely confined to the southeast part of the region in winter, but is highly variable in summer

when the wind patterns are more sporadic. The region west of Vancouver Island lies at the northern end of the California Current upwelling favorable zone which transitions to a downwelling favorable zone to the north. The variability in the location of the transition was part of the reason we chose to define our study regions by implementing a K-means clustering approach.

Clustering allows for a data driven estimate of regions with similar environmental conditions. By using K-means clustering using climatologies of potential temperature, AOU and aragonite saturation state (described in section 2.2 of the manuscript) instead of solely relying on expert knowledge, we reduce dependence on specialized expertise and enhance the scalability and adaptability of this methodology for broader application.

We explored using a different number of clusters and found that 6 clusters gave a reasonable set of coherent regions without an excessive amount of spatially disconnected points in the clusters. Justifying this via a traditional silhouette analysis (Murphy, 2022) (measuring the compactness of the cluster relative to the distance to the neighboring cluster) was not possible due to the strong gradients in the predictors that arise from the topography of continental slope. Essentially, increasing the number of clusters tends to pick out finer contours of the continental slope. The silhouette score thus tends to decrease monotonically as the number of points in each cluster becomes more and more varied. Visually, the Shallows and Canyons clusters do not significantly change when varying the number of clusters from 5 to 9 (not shown).

To measure the impact of the choice of the number of clusters on our analysis, we calculated the thresholds, as described in section 2.3 of the main text, for these different

cluster sizes. We found that the variance of the thresholds is $\leq 10\%$ when using 5 to 9 clusters and $\leq 5\%$ when using 5 to 7 clusters. The number of grid cells and climatological centres for each of the six clusters used here (Figure S6) are shown in Table S3.

For each cluster, a statistical extreme is defined using the distribution of values of dissolved oxygen, temperature and aragonite saturation state (Figure S7). The temporal division into upwelling and downwelling regimes may be unique to eastern boundary upwelling systems, but other features such as the timing of the spring freshet or melting of sea ice may be relevant if generalizing this method to other systems. The difference in the distributions for upwelling and downwelling seasons is more pronounced for the Shallows (Fig. S7).

Since all of the clusters depend on bottom depth, it's not surprising that the resulting clusters are associated with specific depth ranges (Fig. S6). Even though the clusters have some overlapping depths, they occupy unique positions in the 3D environmental space (Table S3). The two clusters selected for presentation in the paper are the Shallows (Fig. S6 d) and the Canyons (Fig. S6 a) as described in Section 2.2 and 3.1 of the main text.

Given the strong dependence of these clusters on the bottom depth, we also consider using a simpler method of grouping the benthic regions by depth. To demonstrate that clustering does a better job of identifying regions with similar environmental characteristics we found the deepest depth in the Shallows ($\simeq 69\,\mathrm{m}$) and extracted all of the grid cells with bottom depths shallower than that depth. Comparing the locations in 3D parameter space demonstrates that the depth delineation results in a much wider range of values

(yellow diamonds in Fig. S8 (b)) for each of the three potential stressors. Many, but not all, of the points in the depth defined region are located on West Coast Vancouver Island. We plotted orange crosses to indicate the parameter space of the points (depths $< 69\,\mathrm{m}$) north of $51^\circ\,\mathrm{N}$ which shows that temperature, AOU and Ω_A can vary significantly at the same depth (Fig. S8 (b)). A data driven approach using machine learning to cluster the data takes the guesswork out of defining regions with similar characteristics.

Given that the goal of this paper is to study extremes, we investigated the role that temporal resolution of the data could have on the calculated thresholds. Benthic temperature was saved at 3-hour resolution. Thresholds for the Shallows and Canyons regions were calculated with 3-hour, 6-hour, 12-hour, daily, and five day averaging windows. For both the Shallows and the Canyons, during upwelling and downwelling, all resulting thresholds were within 0.01°C of each other. The only exception was the Shallows cluster during downwelling season where the threshold dropped by 0.1°C between the daily and five day averages. Therefore, we chose to limit our analysis to daily averages.

Text S3: Occurrence of extremes over time

The occurrence of extremes over time is discussed in detail in section 3.2 of the manuscript. This section provides supporting information for the compound extremes, analysis of trends, and event duration for the Shallows and Canyons and provides a brief overview of our analysis for the remaining clusters.

A compound extreme is defined here as the concomitant occurrence of two or more stressors in the same grid cell. We show all of the compound extremes for the Canyons (Figure S9) and the Shallows (Figure S10) clusters, but only the triple extremes for the

remaining clusters (Figure S11). The most common compound extreme were coincident extremes in $[O_2]$ and Ω_A.

Some of the clusters (b, d, e, f) exhibit an increasing number of triple extremes near the end of the time series (Fig. S11), while the clusters with the deepest average depths do not (Table S3). For these deeper clusters the maximum depth of the mixed layer is typically much shallower than the ocean bottom. With less ventilation, these deeper clusters will not experience the increase in anthropogenic CO_2 emissions as immediately as the shallower clusters, nor will they immediately feel the effects of near-surface marine heatwaves. However, the deeper clusters shown in Fig. S6 (c, a, and e (from deepest to shallowest)) have waters with Ω_A at or below saturation ($\Omega_A < 1$) and relatively low oxygen as a baseline (Table S3), so organisms in these regions may be particularly vulnerable to extremes in Ω_A and $[O_2]$. In particular, cluster 'e', where groundfish biodiversity is high (Thompson et al., 2023), has baseline conditions near ecological thresholds and the deepest annual mixed layer depths are comparable with the ocean bottom depth. Triple stressor extremes are more frequent in this cluster because it is influenced by both upwelling and surface ocean extremes, especially at the end of the time series.

We analyzed the trends in single and compound extremes using linear regression and accounting for autocorrelation in the time series by calculating the effective sample size

$$N_{eff} = N\frac{1 - r_1}{1 + r_1}$$

where r_1 is the lag-one autocorrelation (Bretherton et al., 1999). The only statistically significant trend (p$>$ 0.05) in the single stressor extremes was for Ω_A extremes in the Shallows with the fraction of extreme waters increasing by about $0.004\,\mathrm{y}^{-1}$. Clusters 'b',

'd' and 'e' all exhibited significant trends for triple extremes, which increased at rates of $2 \times 10^{-4}\,\mathrm{y}^{-1}$, $3 \times 10^{-5}\,\mathrm{y}^{-1}$, and $3 \times 10^{-4}\,\mathrm{y}^{-1}$, respectively. All three also exhibited significant trends for O_2/T extremes with similar rates, and clusters 'b' and 'd' exhibited increasing trends for Ω_A/T extremes.

The duration of an extreme event was calculated for each grid cell, and the maximum values averaged for each cluster (Table 1 of the main text). The average duration is longer for temperature than for O_2 and Ω_A in the Canyons, while the opposite is true in the Shallows. Differences between the upwelling and downwelling seasons are generally small, but the longest duration events are in the Canyons during the downwelling season.

Text S4: The influence of basin scale climate variability

Climate Indices

Extreme conditions of hypoxia and acidification in the Canadian North Pacific are strongly influenced by changes in upwelling along the continental shelf and the ocean's stratification and temperature. Hence, we examine the relationship between the fraction of extremes and four climate indices which are associated with variability in these conditions: the Multivariate ENSO Index (MEI), the Pacific Decadal Oscillation (PDO), The North Pacific Gyre Oscillation (NPGO) and the Bakun upwelling index (Figure S12). It is important to recognize that these indices are influenced by many processes. They are briefly described in this section.

The El Niño–Southern Oscillation (ENSO) is a recurring pattern of climate variability originating in the tropical Pacific and propagating into the exratropics by a variety of mechanisms. Different indices are used to characterize the phases of ENSO (e.g., NINO3,

NINO4, SOI). For the present study ENSO is represented using the Multivariate ENSO Index version 2 (MEI) which uses five variables from the JRA-55 reanalysis (Kobayashi et al., 2015) over the tropical Pacific basin (30°S − 30°N and 100°E − 70°W): sea level pressure, sea surface temperature, surface zonal and meridional wind, and outgoing longwave radiation (NOAA Physical Sciences Laboratory, 2024). This index captures all of the ENSO events of the other indices and has the advantages that it does not rely on a single station or variable.

The Pacific Decadal Oscillation (PDO) is a pattern of North Pacific (20°-70°N) Sea Surface Temperature (SST) variability. It is the leading principal component of North Pacific SST anomalies (Mantua & Hare, 2002). The warm phase is characterized by warm ocean waters along the west coast of North America coincident with anomalously cool SSTs in the central North Pacific. The opposite pattern is observed in the cool phase. These patterns are influenced by a combination of processes (e.g., Aleutian Low) operating on different time-scales (Newman et al., 2016). The index used for this study was based on ERSSTv5, but similar results are obtained for this period using other SST datasets (Newman et al., 2016; Huang et al., 2017; NOAA Physical Sciences Laboratory, 2022).

The North Pacific Gyre Oscillation (NPGO) is defined as the second principal component of the sea surface height anomaly (SSHa) over 180°W–110°W; 25°N–62°N (Di Lorenzo et al., 2008; Di Lorenzo, 2022). The SSHa and SSTa fields are highly correlated, hence, as the first and second principal components the PDO and NPGO explain the highest and second highest fraction of the variance in these fields. The NPGO is

associated with upwelling in the CCS because strengthening of the North Pacific Gyre drives more onshore flow as it flow west to east and increases Ekman transport as it flows southward in the California Current resulting in increased upwelling of low oxygen, low pH, and relatively cold water.

We used the Bakun index calculated using Sea Level Pressure on a 3° grid at 48°N, 125°W, and 51°N, 131°W (Bakun, 1973; NOAA Pacific Fisheries Environmental Laboratory, 2022). Although newer upwelling indices have been introduced, they are not appreciably different from the Bakun index at these latitudes (Jacox et al., 2018).

These indices are related to each other by the underlying processes that influence them. ENSO has been dynamically linked to the PDO (Alexander et al., 2002) through a mechanism known as an *atmospheric bridge*; ENSO excites atmospheric teleconnections in the extra-tropics influencing the variability of the Aleutian Low which, in turn, influences the PDO. Similarly, the Central Pacific Warming El Niño pattern drives atmospheric teleconnections in the central North Pacific which results in the NPGO pattern through the North Pacific Oscillation (NPO) (Di Lorenzo et al., 2023).

Correlations with the climate indices

There is reason to believe that these climate indices may have predictive power for local ecosystem changes along the continental margin of British Columbia. For example, large shifts in zooplankton taxa around Vancouver Island Mackas, Peterson, and Zamon (2004) and in the California Current system (Mackas et al., 2006) were associated with ENSO and Pacific regime shifts, Mackas et al. (2013) found that zooplankton variability in the Strait of Georgia was significantly correlated with the NPGO, Li et al. (2013) found

that the best indicator of zooplankton community change in the Strait of Georgia was the Southern Oscillation Index, Perry and Masson (2013) found that the NPGO was a leading indicator for regime shifts, Perry et al. (2021) found that the PDO was significantly related to zooplankton trends from 1996 to 2018, and Suchy, Young, Galbraith, Perry, and Costa (2022) found a significant relationship between the NPGO and the spring phytoplankton bloom.

We generated monthly averages (bi-monthly for MEI) of the time series of the fraction of extremes by combining the two different seasons. Then, we removed the seasonal cycle and normalized the datasets by subtracting the mean before calculating the cross-correlations. The cross-correlations were computed for a series of lags to better understand the temporal relationships between the variables. We computed the Pearson Correlation Coefficients (Figure S13) and, because these data may not be independent in time, we adjusted the values of p and computed the confidence intervals by considering the equivalent sample size (Von Storch & Zwiers, 2002). Assuming both signals X_i of length N are red-noise (Markov) processes the equivalent sample size is given by

$$N_{eff} = N\frac{1 - r_1 r_2}{1 + r_1 r_2}$$

where r_i is the lag-one autocorrelation for each signal (Bartlett, 1935; Bretherton et al., 1999).

The positive phase of the PDO and ENSO, and the negative phase of the NPGO, are associated with warm near-surface temperatures in the California Current System (CCS) (Di Lorenzo et al., 2008; Chhak et al., 2009) which explains why we found significant positive (negative) correlations between T extremes in the Shallows and MEI and PDO

(NPGO) (Figure S13 a, and Fig. S12 (a, b, c)). Moreover, Amaya et al. (2023) demonstrated that ENSO influences ocean temperature extremes for the Canadian west coast via coastally trapped waves. Similar correlations were found for low oxygen extremes, indicating the strong influence of solubility on oxygen extremes for this cluster (Fig. S13 a). Extremes in Ω_A are negatively correlated with the PDO. The warm phase of the PDO is associated with greater stratification and a deeper thermocline, resulting in less penetration of old, corrosive and oxygen-poor waters onto the continental margin.

In the Canyons, $[O_2]$ and Ω_A extremes both exhibit a negative correlation with the PDO and a positive correlation with the NPGO (Figure S13); both indices are associated with upwelling. The only significant correlation with the Bakun index was for temperature in the Canyons, but the correlation was weaker than those for the climate indices. The Bakun index represents the strength of upwelling/downwelling due to changes in the local winds (inferred from SLP), but other processes can contribute to upwelling in the Northern CCS (Engida et al., 2016). For example, coastally trapped waves (CTW) are excited by wind stress far to the south and propagate along the coast. They depress the thermocline, modify upwelling and influence all three stressors (Engida et al., 2016). Overall the effects of large-scale climate variability are more readily detectable in our data set than those of locally forced upwelling.

References

Alexander, M. A., Bladé, I., Newman, M., Lanzante, J. R., Lau, N.-C., & Scott, J. D. (2002). The atmospheric bridge: The influence of ENSO teleconnections on air–sea interaction over the global oceans. *Journal of Climate*, *15*(16), 2205 - 2231. doi:

10.1175/1520-0442(2002)015⟨2205:TABTIO⟩2.0.CO;2

Amaya, D. J., Jacox, M. G., Alexander, M. A., Scott, J. D., Deser, C., Capotondi, A., & Phillips, A. S. (2023). Bottom marine heatwaves along the continental shelves of North America. *Nature Communications*, *14*(1), 1038. doi: DOI={10.1038/s41467-023-36567-0}

Bakun, A. (1973). Coastal upwelling indices, west coast of North America, 1946-71 [NOAA Technical Report NMFS SSRF-671].

Bartlett, M. (1935). Some aspects of the time-correlation problem in regard to tests of significance. *Journal of the Royal Statistical Society*, *98*(3), 536–543. doi: 10.2307/2342284

Bianucci, L., Denman, K. L., & Ianson, D. (2011). Low oxygen and high inorganic carbon on the vancouver island shelf. *Journal of Geophysical Research: Oceans*, *116*(C7). doi: 10.1029/2010JC006720

Bretherton, C. S., Widmann, M., Dymnikov, V. P., Wallace, J. M., & Bladé, I. (1999). The effective number of spatial degrees of freedom of a time-varying field. *Journal of climate*, *12*(7), 1990–2009. doi: 10.1175/1520-0442(1999)012⟨1990:TENOSD⟩2.0.CO;2

Chhak, K. C., Di Lorenzo, E., Schneider, N., & Cummins, P. F. (2009). Forcing of low-frequency ocean variability in the northeast Pacific. *Journal of Climate*, *22*(5), 1255–1276. doi: 10.1175/2008JCLI2639.1

Chisholm, S. W. (1992). Phytoplankton size. In P. G. Falkowski & A. D. Woodhead (Eds.), *Primary productivity and biogeochemical cycles in the sea* (pp. 213–237).

Plenum. doi: 10.1007/978-1-4899-0762-2_12

Christian, J. R., Denman, K. L., Hayashida, H., Holdsworth, A. M., Lee, W. G., Riche, O. G., ... Swart, N. C. (2022). Ocean biogeochemistry in the Canadian Earth system model version 5.0.3: CanESM5 and CanESM5-CanOE. *Geoscientific Model Development*, *15*(11), 4393–4424. doi: 10.5194/gmd-15-4393-2022

Cummins, P. F., & Oey, L.-Y. (1997). Simulation of barotropic and baroclinic tides off northern British Columbia. *Journal of Physical Oceanography*, *27*(5), 762–781. doi: 10.1175/1520-0485(1997)027⟨0762:SOBABT⟩2.0.CO;2

Denman, K., & Pena, M. (2002). The response of two coupled one-dimensional mixed layer/planktonic ecosystem models to climate change in the NE subarctic Pacific ocean. *Deep Sea Research Part II: Topical Studies in Oceanography*, *49*(24-25), 5739–5757. doi: 10.1016/S0967-0645(02)00212-6

Department of Fisheries and Oceans Canada (DFO). (2022). *Institute of Ocean Sciences Data Archive* [Data set]. (Data obtained on 2022/05/15 from `www.waterproperties.ca`)

Devol, A. H. (1991). Direct measurement of nitrogen gas fluxes from continental shelf sediments. *Nature*, *349*(6307), 319-321. doi: 10.1038/349319a0

Devol, A. H., & Christensen, J. P. (1993). Benthic fluxes and nitrogen cycling in sediments of the continental margin of the eastern north Pacific. *Journal of Marine Research*, *51*(2), 345-372. doi: 10.1357/0022240933223765

Di Lorenzo, E. (2022). *The North Pacific Gyre Oscillation (NPGO)* [Data set]. (Data obtained on 11/25/2022 from `https://www.o3d.org/npgo/data/NPGO.txt`)

Di Lorenzo, E., Schneider, N., Cobb, K. M., Franks, P. J. S., Chhak, K. C., Miller, A. J., ... Rivière, P. (2008). North Pacific Gyre Oscillation links ocean climate and ecosystem change. *Geophysical Research Letters*, *35*(8). doi: 10.1029/2007GL032838

Di Lorenzo, E., Xu, T., Zhao, Y., Newman, M., Capotondi, A., Stevenson, S., ... others (2023). Modes and mechanisms of Pacific decadal-scale variability. *Annual Review of Marine Science*, *15*(1), 249–275. doi: 10.1146/annurev-marine-040422-084555

Engida, Z., Monahan, A., Ianson, D., & Thomson, R. E. (2016). Remote forcing of subsurface currents and temperatures near the northern limit of the California Current system. *Journal of Geophysical Research: Oceans*, *121*(10), 7244–7262. doi: 10.1002/2016JC011880

Fennel, K., Wilkin, J., Levin, J., Moisan, J., O'Reilly, J., & Haidvogel, D. (2006). Nitrogen cycling in the Middle Atlantic Bight: Results from a three-dimensional model and implications for the North Atlantic nitrogen budget. *Global Biogeochemical Cycles*, *20*(3). doi: 10.1029/2005GB002456

Heip, C., Duineveld, G., Flach, E., Graf, G., Helder, W., Herman, P., ... others (2001). The role of the benthic biota in sedimentary metabolism and sediment-water exchange processes in the Goban Spur area (NE Atlantic). *Deep Sea Research Part II: Topical Studies in Oceanography*, *48*(14), 3223-3243. doi: 10.1016/S0967-0645(01)00038-8

Holdsworth, A. M., Zhai, L., Lu, Y., & Christian, J. R. (2021). Future changes in oceanography and biogeochemistry along the Canadian Pacific continental margin. *Frontiers in Marine Science*, *8*. doi: 10.3389/fmars.2021.602991

Holte, J., & Talley, L. (2009). A new algorithm for finding mixed layer depths with applications to Argo data and Subantarctic mode water formation. *Journal of Atmospheric and Oceanic Technology*, *26*(9), 1920–1939. doi: 10.1175/2009JTECHO543.1

Huang, B., Thorne, P. W., Banzon, V. F., Boyer, T., Chepurin, G., Lawrimore, J. H., ... others (2017). NOAA extended reconstructed sea surface temperature (ERSST), version 5. *NOAA National Centers for Environmental Information*, *30*, 8179–8205.

Humphreys, M. P., Lewis, E. R., Sharp, J. D., & Pierrot, D. (2022). Pyco2sys v1. 8: Marine carbonate system calculations in python. *Geoscientific Model Development*, *15*(1), 15–43. doi: 10.5194/gmd-15-15-2022

Jacox, M. G., Edwards, C. A., Hazen, E. L., & Bograd, S. J. (2018). Coastal upwelling revisited: Ekman, Bakun, and improved upwelling indices for the us west coast. *Journal of Geophysical Research: Oceans*, *123*(10), 7332–7350. doi: 10.1029/2018JC014187

Kling, H., Fuchs, M., & Paulin, M. (2012). Runoff conditions in the upper Danube basin under an ensemble of climate change scenarios. *Journal of Hydrology*, *424-425*, 264-277. doi: 10.1016/j.jhydrol.2012.01.011

Knoben, W. J., Freer, J. E., & Woods, R. A. (2019). Inherent benchmark or not? comparing Nash–Sutcliffe and Kling–Gupta efficiency scores. *Hydrology and Earth System Sciences*, *23*(10), 4323–4331. doi: 10.5194/hess-23-4323-2019

Kobayashi, S., Ota, Y., Harada, Y., Ebita, A., Moriya, M., Onoda, H., ... Takahashi, K. (2015). The JRA-55 Reanalysis: General specifications and basic characteristics. *Journal of the Meteorological Society of Japan. Ser. II*, *93*(1), 5-48. doi: 10.2151/jmsj.2015-001

Li, L., Mackas, D., Hunt, B., Schweigert, J., Pakhomov, E., Perry, R. I., ... Pitcher, T. J. (2013). Zooplankton communities in the Strait of Georgia, British Columbia, track large-scale climate forcing over the Pacific Ocean. *Progress in Oceanography*, *115*, 90–102. doi: 10.1016/j.pocean.2013.05.025

Lyard, F. H., Allain, D. J., Cancet, M., Carrère, L., & Picot, N. (2021). FES2014 global ocean tide atlas: design and performance. *Ocean Science*, *17*(3), 615–649.

Mackas, D., Galbraith, M., Faust, D., Masson, D., Young, K., Shaw, W., ... Sastri, A. (2013). Zooplankton time series from the Strait of Georgia: Results from year-round sampling at deep water locations, 1990–2010. *Progress in Oceanography*, *115*, 129–159. doi: 10.1016/j.pocean.2013.05.019

Mackas, D., Peterson, W., Ohman, M., & Lavaniegos, B. (2006). Zooplankton anomalies in the California Current system before and during the warm ocean conditions of 2005. *Geophysical Research Letters*, *33*(22). doi: 10.1029/2006GL027930

Mackas, D., Peterson, W., & Zamon, J. (2004). Comparisons of interannual biomass anomalies of zooplankton communities along the continental margins of British Columbia and Oregon. *Deep Sea Research Part II: Topical Studies in Oceanography*, *51*(6-9), 875–896. doi: 10.1016/j.dsr2.2004.05.011

Mantua, N. J., & Hare, S. R. (2002). The Pacific Decadal Oscillation. *Journal of oceanography*, *58*(1), 35–44. doi: 10.1023/A:1015820616384

Murphy, K. P. (2022). *Probabilistic machine learning: An introduction*. The MIT Press.

Newman, M., Alexander, M. A., Ault, T. R., Cobb, K. M., Deser, C., Lorenzo, E. D., ... Smith, C. A. (2016). The Pacific Decadal Oscillation, revisited. *Journal of Climate*,

29(12), 4399 - 4427. doi: 10.1175/JCLI-D-15-0508.1

NOAA Pacific Fisheries Environmental Laboratory. (2022). *Traditional 3 degree Bakun index* [Data set]. National Oceanic and Atmospheric Administration. (Data obtained on 03/10/2022 from `oceanwatch.pfeg.noaa.gov/products/PFELData/upwell/monthly/upindex.mon`)

NOAA Physical Sciences Laboratory. (2022). *The Pacific Decadel Oscillation (PDO)* [Data set]. National Oceanic and Atmospheric Administration. (Data obtained on 12/16/2022 from `https://psl.noaa.gov/pdo/`)

NOAA Physical Sciences Laboratory. (2024). *Multivariate ENSO Index Version 2 (MEI.v2)* [Data set]. National Oceanic and Atmospheric Administration. (Data obtained on 01/11/2024 from `https://www.psl.noaa.gov/enso/mei`)

NRCan. (2022). *Geodetic reference systems* [Data set]. Natural Resources Canada. (`https://www.nrcan.gc.ca/maps-tools-and-publications/tools/geodetic-reference-systems/canadian-spatial-reference-system-csrs/9052#cgvd28`)

Perry, R. I., & Masson, D. (2013). An integrated analysis of the marine social–ecological system of the Strait of Georgia, Canada, over the past four decades, and development of a regime shift index. *Progress in Oceanography*, *115*, 14–27. doi: 10.1016/j.pocean.2013.05.021

Perry, R. I., Young, K., Galbraith, M., Chandler, P., Velez-Espino, A., & Baillie, S. (2021). Zooplankton variability in the Strait of Georgia, Canada, and relationships with the marine survivals of Chinook and Coho salmon. *Plos one*, *16*(1), e0245941.

doi: 10.1371/journal.pone.0245941

Redfield, A. C. (1963). The influence of organisms on the composition of seawater. *The sea*, *2*, 26–77.

Roberts, W., Williams, G. P., Jackson, E., Nelson, E. J., & Ames, D. P. (2018). Hydrostats: A python package for characterizing errors between observed and predicted time series. *Hydrology*, *5*(4). Retrieved from https://www.mdpi.com/2306-5338/5/4/66 doi: 10.3390/hydrology5040066

Sarmiento, J. L., & Gruber, N. (2006). *Ocean Biogeochemical Dynamics*. Princeton: Princeton University Press. doi: 10.1515/9781400849079

Schmidtko, S., Johnson, G. C., & Lyman, J. M. (2013). MIMOC: A global monthly isopycnal upper-ocean climatology with mixed layers. *Journal of Geophysical Research: Oceans*, *118*(4), 1658–1672. doi: 10.1002/jgrc.20122

Seitzinger, S. P., & Giblin, A. E. (1996). Estimating denitrification in North Atlantic continental shelf sediments. In *Nitrogen cycling in the North Atlantic ocean and its watersheds* (pp. 235–260). Springer. doi: 10.1007/BF02179829

Soetaert, K., Middelburg, J. J., Herman, P. M., & Buis, K. (2000). On the coupling of benthic and pelagic biogeochemical models. *Earth-Science Reviews*, *51*(1-4), 173–201. doi: 10.1016/S0012-8252(00)00004-0

Suchy, K. D., Young, K., Galbraith, M., Perry, R. I., & Costa, M. (2022). Match/mismatch between phytoplankton and crustacean zooplankton phenology in the Strait of Georgia, Canada. *Frontiers in Marine Science*, *9*, 832684. doi: 10.3389/fmars.2022.832684

Thompson, P. L., Nephin, J., Davies, S. C., Park, A. E., Lyons, D. A., Rooper, C. N., ... Holdsworth, A. M. (2023). Groundfish biodiversity change in northeastern Pacific waters under projected warming and deoxygenation. *Philosophical Transactions of the Royal Society B: Biological Sciences*, *378*(1881), 20220191. doi: 10.1098/rstb.2022.0191

Thomson, R. (1981). Oceanography of the British Columbia coast. Canadian special publication of fisheries and aquatic science. *Fisheries and Oceans Canada*, 291.

Von Storch, H., & Zwiers, F. W. (2002). *Statistical analysis in climate research*. Cambridge university press.

Wolf-Gladrow, D. A., Zeebe, R. E., Klaas, C., Körtzinger, A., & Dickson, A. G. (2007). Total alkalinity: The explicit conservative expression and its application to biogeochemical processes. *Marine Chemistry*, *106*(1-2), 287–300. (Special issue: Dedicated to the memory of Professor Roland Wollast) doi: 10.1016/j.marchem.2007.01.006

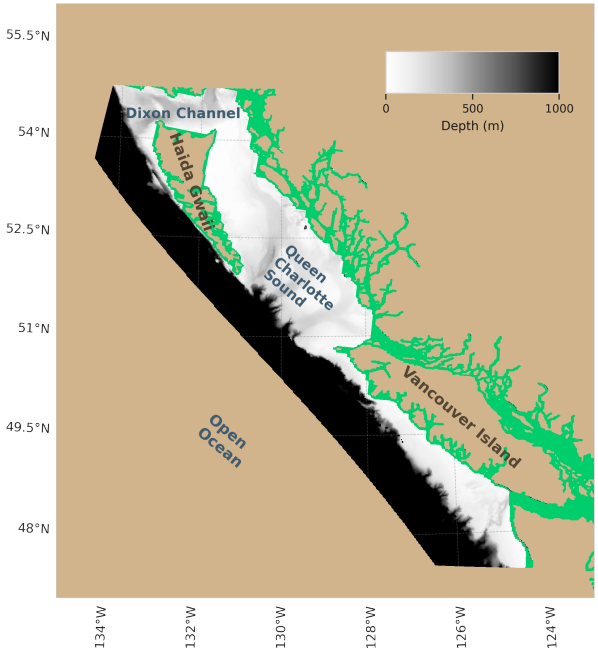

Figure S1. Domain and bathymetery for the analyzed model outputs. Regions excluded from analysis because the of the model's limited resolution are shown in green.

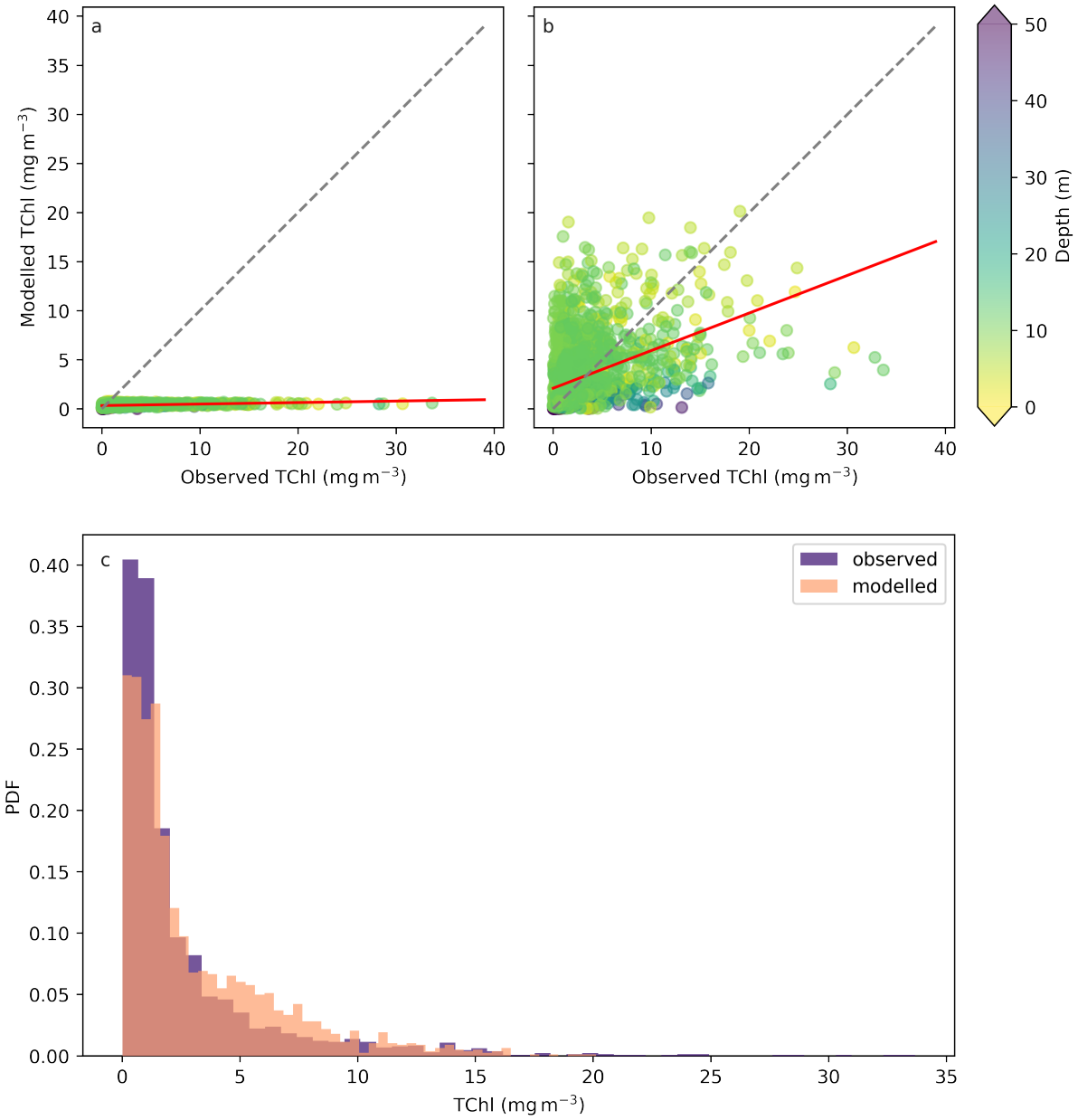

Figure S2. Illustration of the representation of the total chlorophyll in NEP36-CanOE with the (a) evaluation with the parameters originally developed for the global model, (b) the evaluation with the revised parameters for the Northeastern Pacific continental margin, and (c) the probability density function for the observations and revised model. The apparent third color is simply the overlapping of the other two.

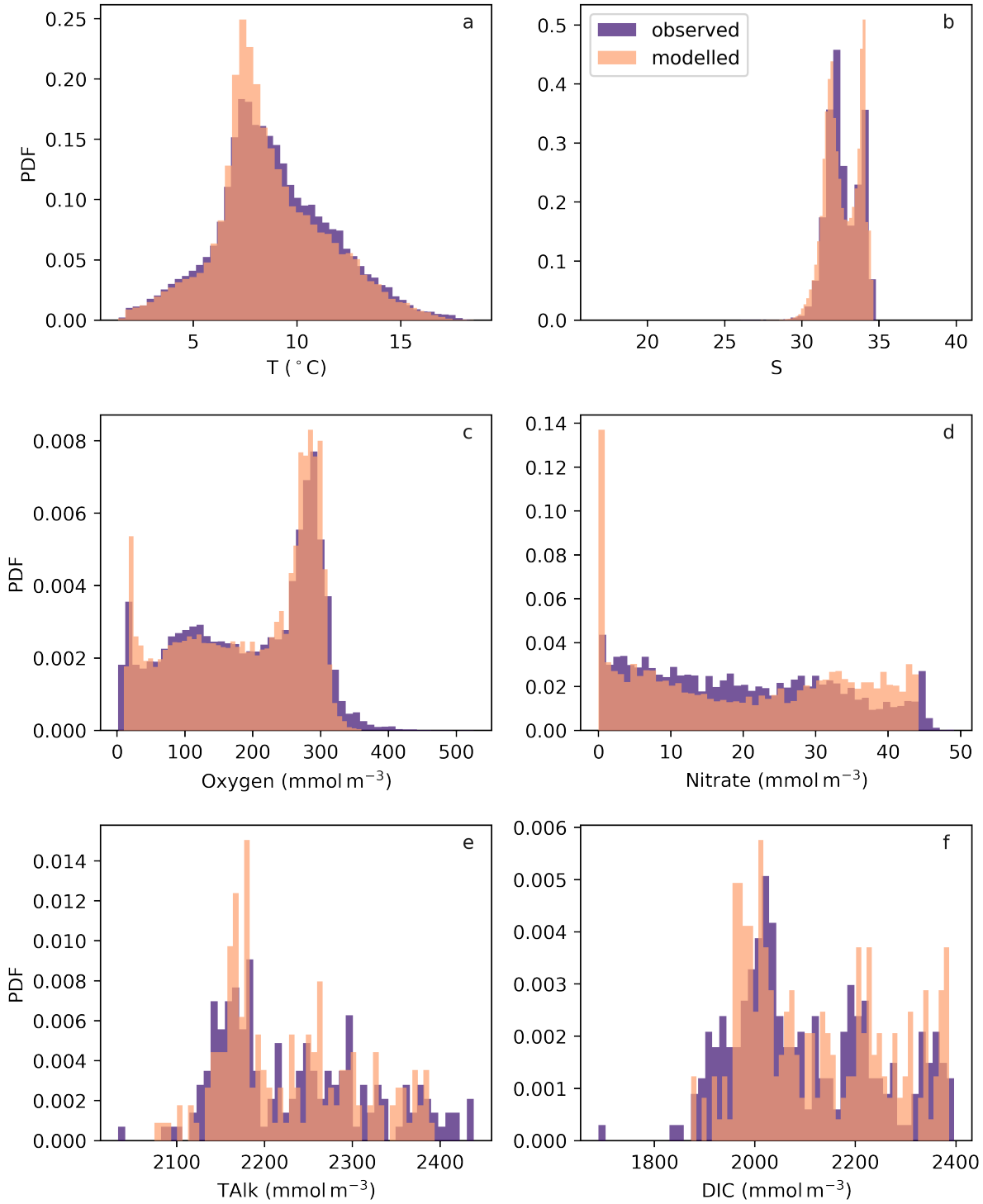

Figure S3. The probability density functions for the ship-sampled observations and modelled (a) potential temperature, (b) salinity, (c) oxygen, (d) nitrate, (e) total alkalinity (f) dissolved inorganic carbon. The apparent third color is simply the overlapping of the other two.

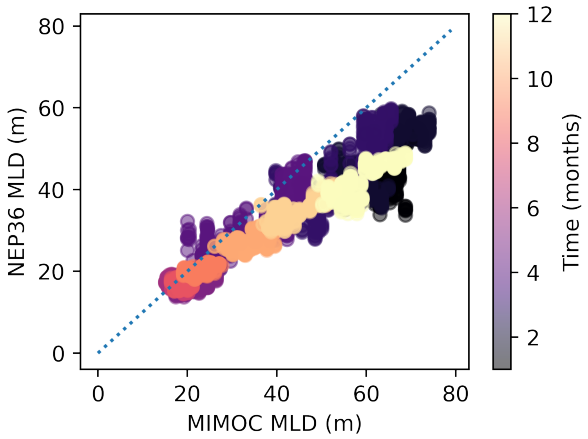

Figure S4. Mixed layer depths from the model plotted against the MIMOC climatology. The colormap shows the months of the year.

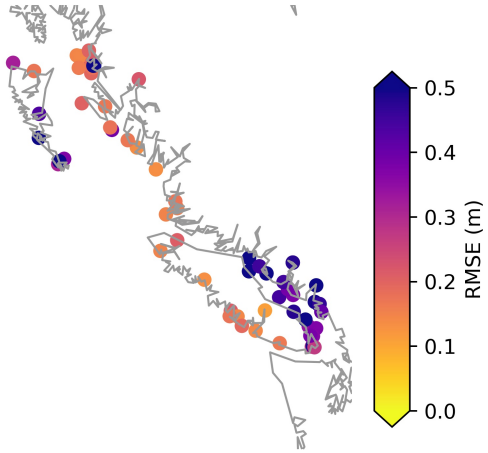

Figure S5. The RMSE of the total water level in the model compared with tide gauge observations.

Table S1. The average bias (model-observations) in the magnitude of the tidal amplitude and phase along with the tidal error associated with significant constituents.

constituent	Amplitude (m)	Phase (°)	Tide (m)
M2	0.10 ± 0.12	19.00 ± 67.72	0.11 ± 0.06
S2	0.03 ± 0.03	6.93 ± 8.52	0.04 ± 0.02
N2	0.02 ± 0.03	80.32 ± 139.90	0.03 ± 0.02
K1	0.11 ± 0.13	12.05 ± 13.79	0.13 ± 0.14
O1	0.05 ± 0.06	12.95 ± 14.37	0.07 ± 0.08
P1	0.04 ± 0.05	12.80 ± 14.00	0.04 ± 0.05
K2	0.005 ± 0.006	6.06 ± 9.29	0.008 ± 0.006

Table S2. Evaluation of model outputs against the observations for several metrics: the signed root mean squared error (RMSE), the Pearson correlation r, the variability ratio α, the bias ratio β and the Kling-Gupta efficiency (KGE), the bias in the 90^{th} percentile of values and the bias in the 10^{th} percentile of values. RMSE and biases (but not bias ratio) have the same units as their respective data fields.

variable	RMSE	r	α	β	KGE	$\text{bias}_{10\text{th}}$	$\text{bias}_{90\text{th}}$
T	-0.80	0.96	0.97	0.98	0.95	.22	**-0.23**
S	-0.4	0.94	1.08	1.00	0.90	-0.18	0.004
O_2	32.2	0.94	0.96	1.00	0.93	**-1.78**	-4.90
NO_3	7	0.89	1.10	1.01	0.85	-1.82	2.24
DIC	51	0.95	0.96	1.01	0.93	32.6	**10.0**
TAlk	-29	0.95	0.88	1.00	0.87	**6.7**	-23.3
TChl	3.3	0.46	0.78	1.03	0.42	-0.13	1.70

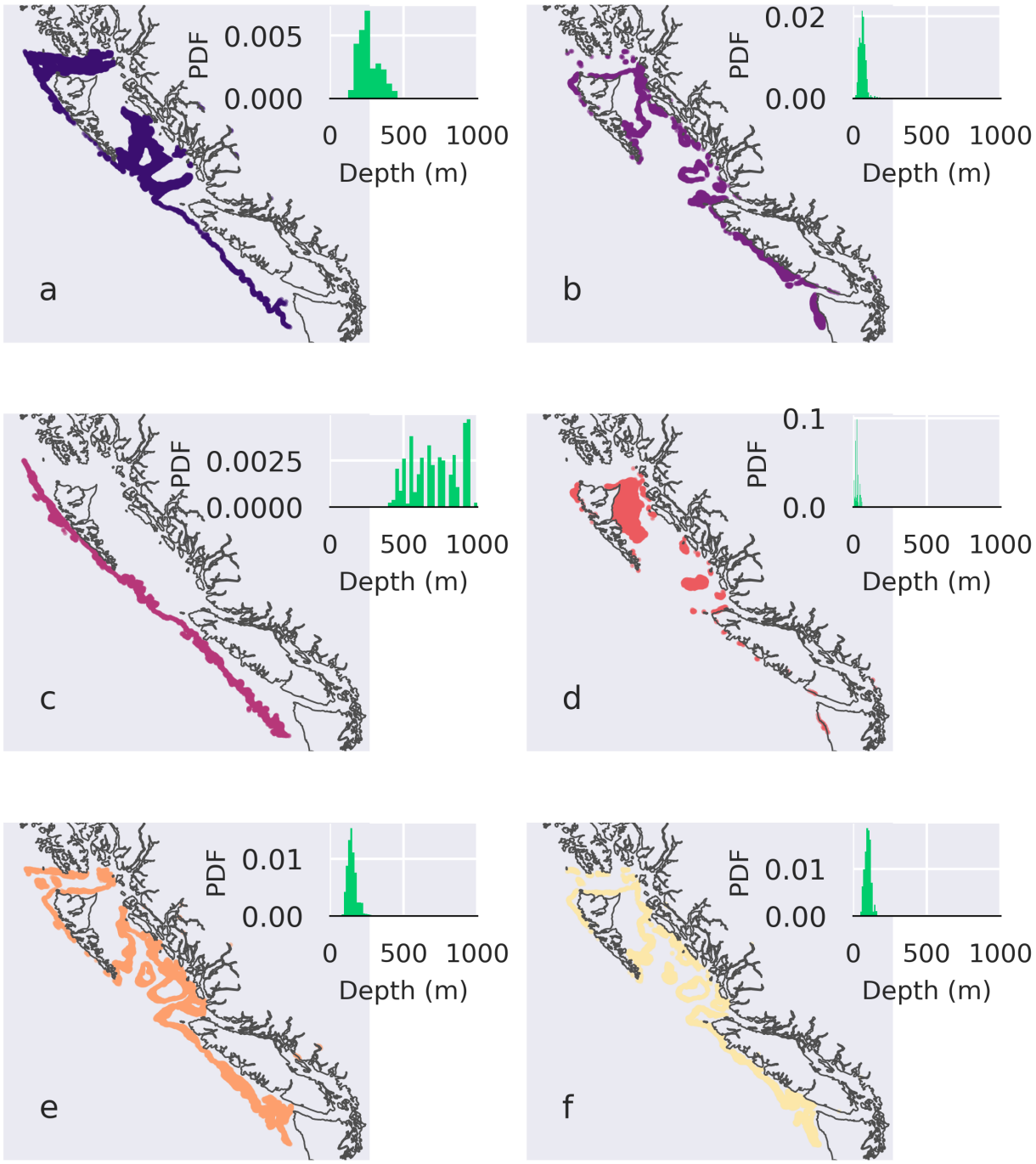

Figure S6. Clusters resulting from applying the K-means algorithm to climatologies of Ω_A, AOU, and T for all bottom depths in the model less than 1000 m. The inset plot shows the distribution of benthic depths for the corresponding cluster. A more detailed description of the methodology is provided in section 2.2 of the manuscript and Text S2.

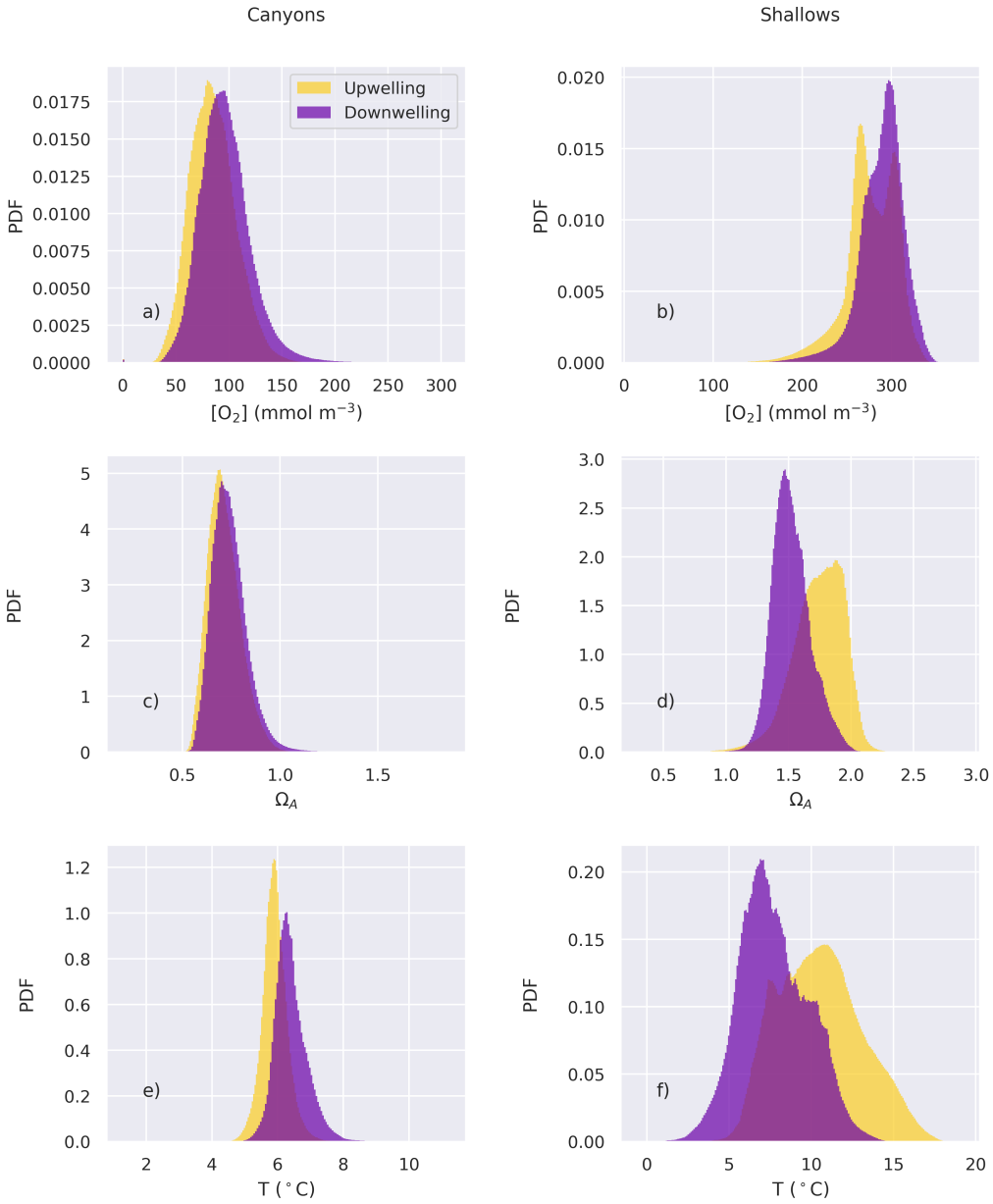

Figure S7. Probability density distributions for the Canyons (left) and Shallows (right) clusters (Fig. S6 a and d, respectively). Dissolved oxygen (a and d), aragonite saturation state (b and e) and temperature (c and f) are shown for each cluster with different colors for upwelling and downwelling seasons. The apparent third color is simply the overlap of the translucent distributions.

Table S3. For the clusters shown in Figure S6, the mean values (climatological centers), average bottom depth and average mixed layer depth (from the daily average data) are shown. The units are °C for T, mmol m^{-3} for AOU and m for depths.

Clusters	grid cells	O_2	AOU	Ω_A	T	bottom depth	MLD_{max}
a	9308	91	211	0.73	6.15	262	165
b	4005	219	71	1.3	8.3	63	74
c	3330	26	288	0.52	4.3	717	135
d	4124	282	5.3	1.63	9.1	29	36
e	7978	122	174	0.84	7.0	151	125
f	5006	168	125	1.04	7.6	101	105

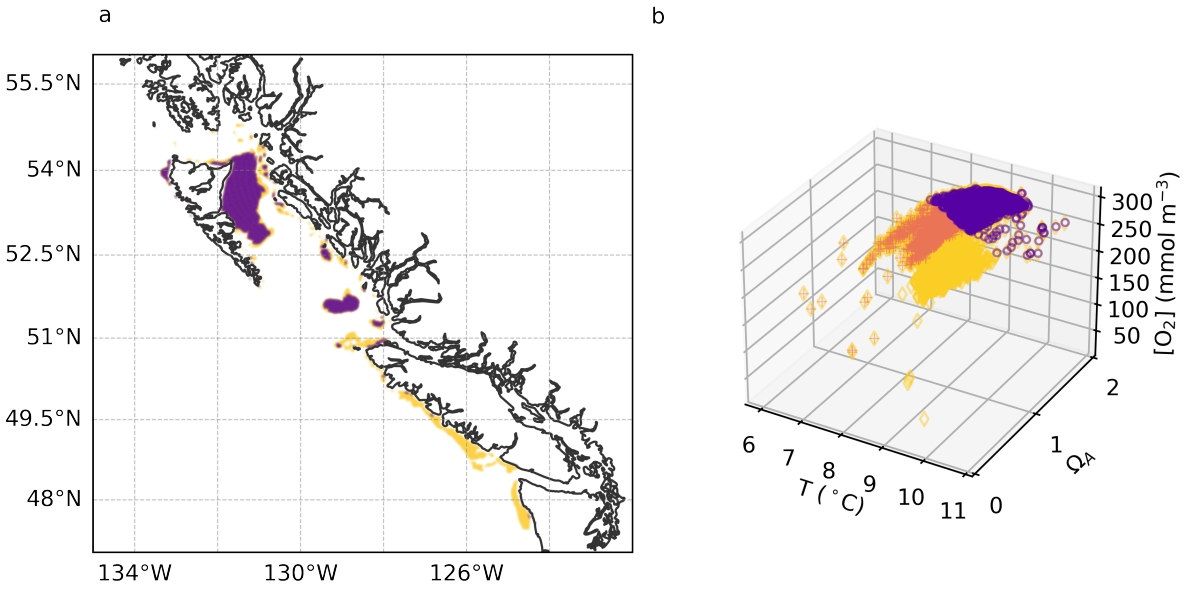

Figure S8. Locations of grid cells in (a) the Shallows cluster (purple) and sub-regions of grid cells with depths less than 69 m (the deepest depth in the Shallows), and (b) their relative positions in 3D parameter space.

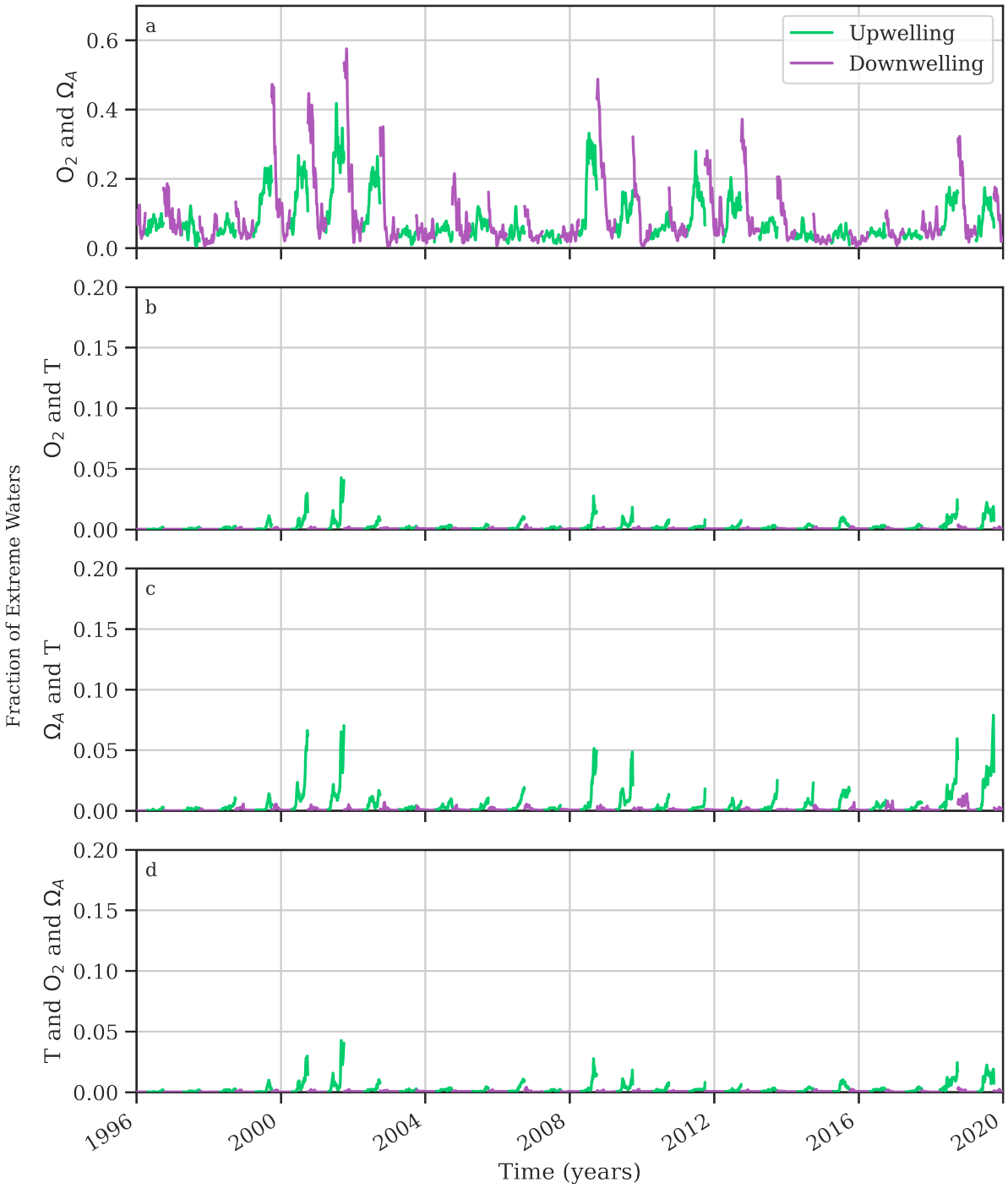

Figure S9. Time series of the fraction of waters in the Canyons cluster (Fig. S6 a) that experience compound extremes in (a) dissolved oxygen and aragonite saturation state, (b) dissolved oxygen and potential temperature, (c) aragonite saturation state and temperature, and (d) temperature, dissolved oxygen and aragonite saturation state.

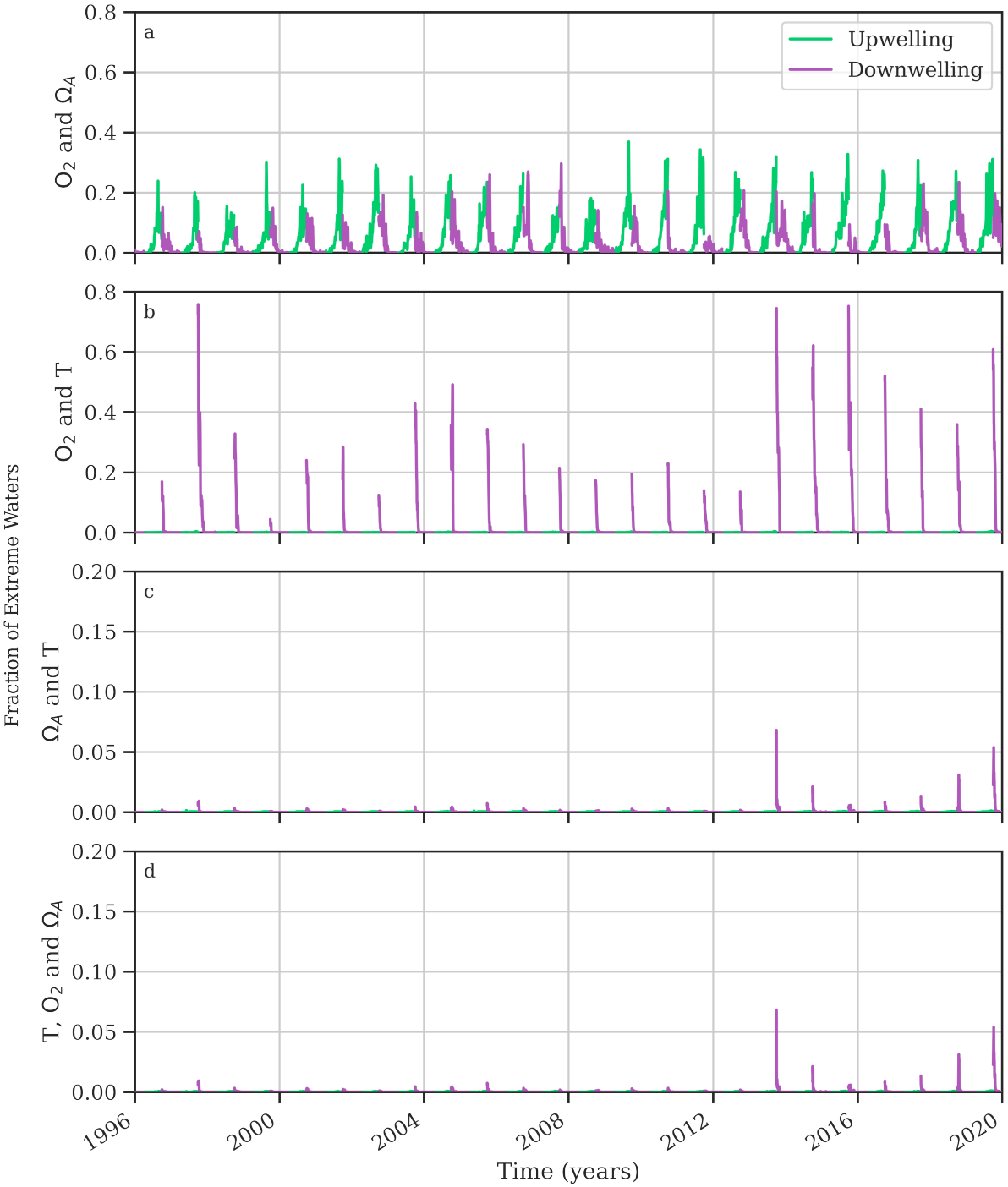

Figure S10. Time series of the fraction of waters in the Shallows cluster (Fig. S6 d) that experience compound extremes in (a) dissolved oxygen and aragonite saturation state, (b) dissolved oxygen and potential temperature, (c) aragonite saturation state and temperature, and (d) temperature, dissolved oxygen and aragonite saturation state.

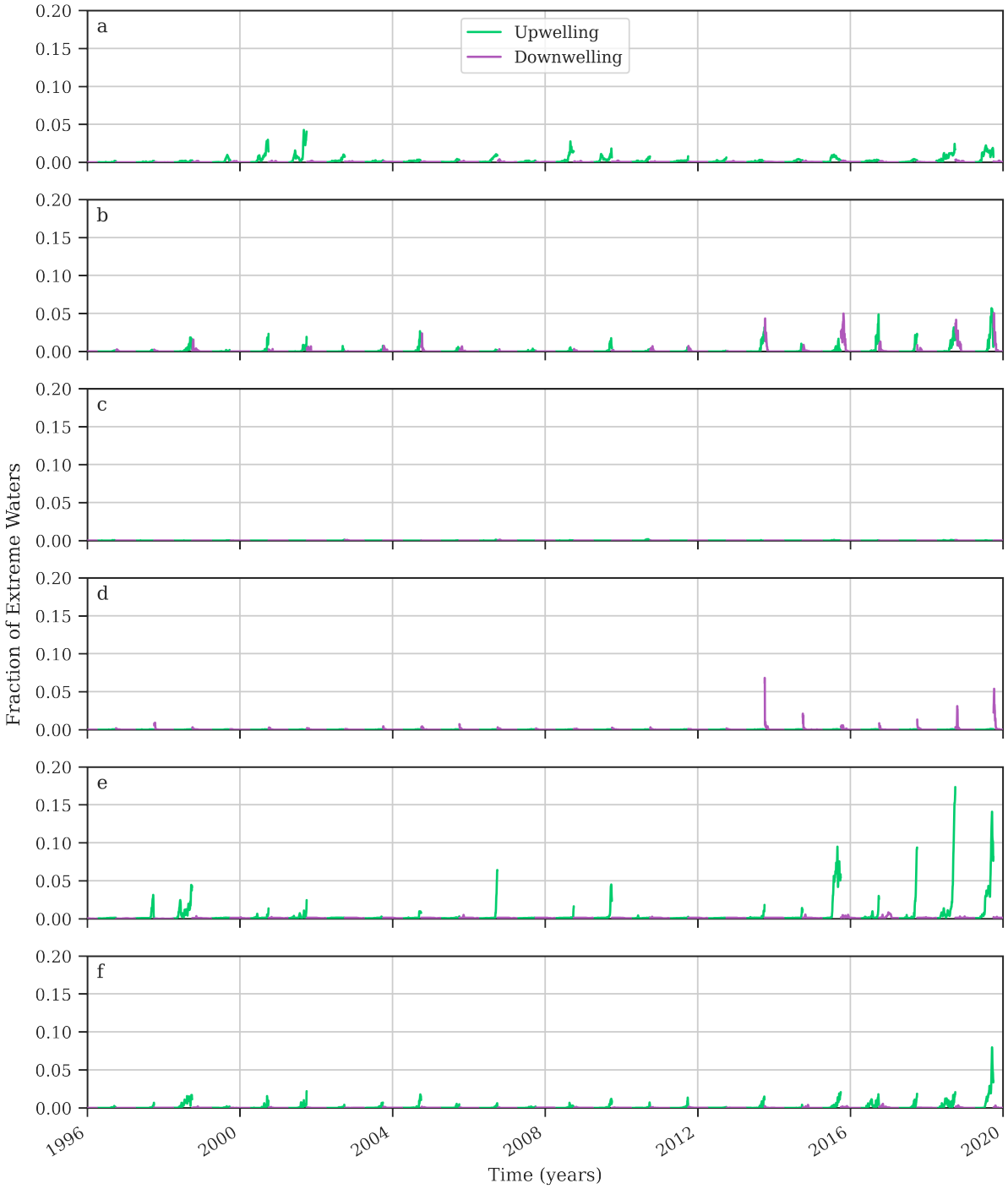

Figure S11. Time series of the fraction of waters that experience extremes in all three stressors (temperature, dissolved oxygen and aragonite saturation state) for all of the clusters in Fig. S6.

Figure S12. Time series of (a) Multivariate ENSO Index (MEI), (b) the Pacific Decadal Oscillation (PDO), (c) The North Pacific Gyre Oscillation (NPGO) and (d) the Bakun upwelling index. The indices are colored red when associated with warm water in the California Current System.

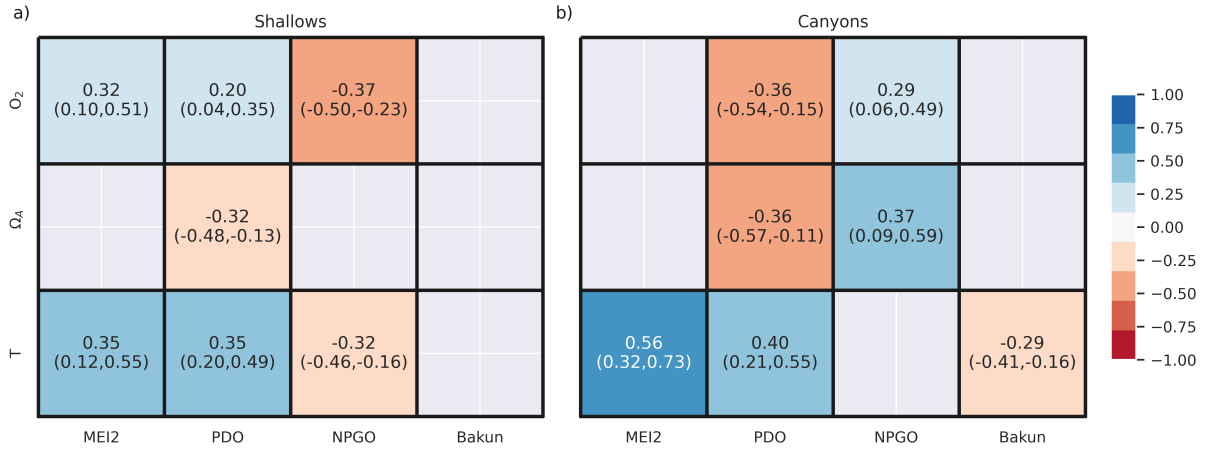

Figure S13. Heatmaps of the correlation between climate indices and the fraction of extreme waters in (a) Shallows and (b) Canyons clusters. The Pearson correlation coefficient is shown along with the 90% confidence interval in parentheses for cases where $p < 0.01$ and the confidence interval does not intersect zero.